TKK Dissertations 179
Espoo 2009

PASSIVELY Q-SWITCHED Nd:YAG LASERS AND THEIR USE IN UV LIGHT GENERATION

Doctoral Dissertation

Ossi Kimmelma

Helsinki University of Technology
Faculty of Electronics, Communications and Automation
Department of Micro and Nanosciences

TKK Dissertations 179
Espoo 2009

PASSIVELY Q-SWITCHED Nd:YAG LASERS AND THEIR USE IN UV LIGHT GENERATION

Doctoral Dissertation

Ossi Kimmelma

Dissertation for the degree of Doctor of Science in Technology to be presented with due permission of the Faculty of Electronics, Communications and Automation for public examination and debate in Auditorium AS2 at Helsinki University of Technology (Espoo, Finland) on the 6th of November, 2009, at 12 noon.

Helsinki University of Technology
Faculty of Electronics, Communications and Automation
Department of Micro and Nanosciences

Teknillinen korkeakoulu
Elektroniikan, tietoliikenteen ja automaation tiedekunta
Mikro- ja nanotekniikan laitos

Distribution:
Helsinki University of Technology
Faculty of Electronics, Communications and Automation
Department of Micro and Nanosciences
P.O. Box 3500 (Tietotie 3)
FI - 02015 TKK
FINLAND
URL: http://nano.tkk.fi/
Tel. +358-9-4511
E-mail: Ossi.Kimmelma@iki.fi

ISBN 978-952-248-073-6
ISBN 978-952-248-074-3 (PDF)
ISSN 1795-2239
ISSN 1795-4584 (PDF)
URL: http://lib.tkk.fi/Diss/2009/isbn9789522480743/

TKK-DISS-2641

Multiprint Oy
Espoo 2009

HELSINKI UNIVERSITY OF TECHNOLOGY
P. O. BOX 1000, FI-02015 TKK
http://www.tkk.fi

ABSTRACT OF DOCTORAL DISSERTATION

Author Ossi Kimmelma

Name of the dissertation

Passively Q-switched Nd:YAG lasers and their use in UV light generation

Date of manuscript 15.05.2009 | Date of the dissertation 6.11.2009

☐ Monograph ☒ Article dissertation (summary + original articles)

Faculty Faculty of Electronics, Communications and Automation
Department Department of Micro and Nanosciences
Field of research Optics
Opponent Prof. Majid Ebrahim-Zadeh
Supervisor Prof. Ilkka Tittonen

Abstract

Recent advances in optoelectronics open up possibilities to realize new kinds of solid state lasers that utilize powerful diode lasers as pump sources. A laser medium has often several appropriate transitions that provide conditions for lasing. Bright pump sources that have recently become available enable building of efficient lasers for wavelengths utilizing such laser transitions that have been unpractical or even totally unattainable.

Pulsed lasers are used to create the intensity needed in the nonlinear conversion. With such a laser, focusing of the light beam into the nonlinear crystal is enough to obtain a decent conversion in the range of a few tens of percents. However, this applies to a laser that is designed to produce high enough peak power for the conversion. In this thesis, passive Q-switching is used to develop high peak power laser sources enabling compact and robust lasers. With these laser sources cascaded frequency conversion using nonlinear processes is demonstrated ranging from IR to deep UV wavelengths.

In this thesis, passively Q-switched Nd:YAG laser crystal was used in lasers putting out pulses at 946, 1064 and 1123 nm. By second harmonic generation these lasers were used in creating light in the visible wavelength range at 473 and 561 nm. By further conversions to UV the wavelengths of 374, 280 and 236 nm were created. At IR wavelengths, peak powers of 3.7 and 3.2 kW at 946 and 1123 nm were achieved, respectively, while the peak powers for the deep UV lasers were 100 and 120 W at wavelengths of 280 and 236 nm, respectively. Tuning of the pulse properties was studied through adjusting the laser crystal temperature in Q-switched Nd:YAG laser at 1064 nm. A remarkable 90 per cent change in peak power was achieved by heating of the laser mount by 100°C with all the studied lasers.

Keywords: solid state lasers, nonlinear optics, passive Q-switching

ISBN (printed) 978-952-248-073-6 | ISSN (printed) 1795-2239
ISBN (pdf) 978-952-248-074-3 | ISSN (pdf) 1795-4584
ISBN (others) | Number of pages 54 p. + app. 34 p.

Publisher Department of Micro and Nanosciences, Helsinki University of Technology

Print distribution Department of Micro and Nanosciences, Helsinki University of Technology

☒ The dissertation can be read at http://lib.tkk.fi/Diss/2009/isbn9789522480743/

TEKNILLINEN KORKEAKOULU PL 1000, 02015 TKK http://www.tkk.fi	VÄITÖSKIRJAN TIIVISTELMÄ

Tekijä Ossi Kimmelma

Väitöskirjan nimi

Passiivisesti Q-kytketyt Nd:YAG laserit ja niiden käyttö UV-valon tuottamisessa

Käsikirjoituksen jättämispäivämäärä 15.05.2009	Väitöstilaisuuden ajankohta 6.11.2009

☐ Monografia ☒ Yhdistelmäväitöskirja (yhteenveto + erillisartikkelit)

Tiedekunta	Elektroniikan, tietoliikennetekniikan ja automaation tiedekunta
Laitos	Mikro- ja nanotekniikan laitos
Tutkimusala	Optiikka
Vastaväittäjä	Prof. Majid Ebrahim-Zadeh
Työn valvoja	Prof. Ilkka Tittonen

Tiivistelmä

Optoelektroniikan viimeaikainen kehitys on tehnyt mahdolliseksi uusien diodipumpattujen kiinteän olomuodon lasereiden realisoinnin. Laservälianeessa on tyypillisesti useita elektronisiirtymiä, jotka soveltuvat käytettäväksi laservahvistuksen aikaansaamiseen. Viime aikoina tarjolle tulleet kirkkaat optiset pumppulähteet mahdollistavat laserlähteiden rakentamisen aallonpituuksille, jotka ovat ennen olleet epäkäytännöllisiä tai jopa kokonaan tavoittamattomissa.

Pulssitetun laserin avulla on mahdollista tuottaa suuri intensiteetti, joka tarvitaan epälineaariseen muunnokseen. Tällaisen laserin avulla fokusointi epälineaariseen kiteeseen riittää kymmenien prosenttien muuntosuhteen saavuttamiseen. Tämä muunnos saadaan kuitenkin vain laserille, joka on suunniteltu tuottamaan riittävän suuri pulssin huipputeho. Tässä työssä passiivista Q-kytkentää on käytetty suuren huipputehon omaavien laserlähteiden kehittämisessä mahdollistaen kompaktin ja kestävän toteutuksen. Näiden lähteiden avulla on demonstroitu valonlähteitä IR-aallonpituuksista aina ultravioletille asti.

Tässä työssä passiivisesti Q-kytkettyä Nd:YAG laseria on käytetty pulssien tuottamiseen aallonpituuksilla 946, 1064 ja 1123 nm. Näkyville aallonpituuksille 473 ja 561 nm on valoa tuotettu käyttäen toisen harmonisen taajuuden tuottamista. Näistä aallonpituuksista edelleen muuntamalla on tuotettu valoa aallonpituuksille 374, 280 ja 236 nm. IR-aallonpituuksilla on saavutettu pulssin huipputehot 3.7 ja 3.2 kW aallonpituuksilla 946 ja 1123 nm kun taas UV aallonpituuksilla 280 ja 236 nm saatiin pulssien huipputehoiksi 100 ja 120 W. Laserpulssin ominaisuuksien muokkausta tutkittiin kontrolloimalla laserkiteen lämpötilaa Q-kytketyllä laserilla aallonpituudella 1064 nm. 100°C lämpötilan muutoksella saatiin aikaan vähintään 90 prosentin muutos huipputehoon kaikilla tutkituilla lasereilla.

Asiasanat: kiinteän olomuodon laserit, epälineaarinen optiikka, passiivinen Q-kytkentä

ISBN (painettu) 978-952-248-073-6	ISSN (painettu) 1795-2239
ISBN (pdf) 978-952-248-074-3	ISSN (pdf) 1795-4584
ISBN (muut)	Sivumäärä 54 s. + liit. 34 s.

Julkaisija Mikro- ja nanotekniikan laitos, Teknillinen korkeakoulu

Painetun väitöskirjan jakelu Mikro- ja nanotekniikan laitos, Teknillinen korkeakoulu

☒ Luettavissa verkossa osoitteessa http://lib.tkk.fi/Diss/2009/isbn9789522480743/

Preface

The work described, in this thesis, was carried out at the Department of Micro and Nanosciences. This work is the culmination of the work that started in the year of 2000 as a students desire to earn some extra while doing something related to the studies. At the time of the Master's thesis the emphasis of the work was however turning strongly towards field that was quite far from anything that would be very familiar for a young electricity student: optics. With Dr. Scott Buchter the research continued on nonlinear optics but also lasers came into the picture. The research on periodical poling was finally successful, but did not result in any published articles. Luckily the study of lasers combined with the experience in nonlinear optics turned out fruitful.

I am grateful to professor Ilkka Tittonen for the opportunity to research this intriguing field and for believing that some day I would make it this far even at times when it wasn't that clear for myself. I thank all the present and former members of our group for relaxed working atmosphere: especially Miika Heiliö for leading to the secrets of electronics, Nikolai Chekurov, group's PR person, for showing the positive power of pessimism and Päivi Sievilä for persistent and dutiful co-operation even with projects that appeared to be impossible.

I am grateful for downstairs optics people for welcoming me into the gang, interesting discussions, good coffee and help with both experiments and theory. Special thanks goes to Klas Lindfors for concentrating on the important and help on various fields; to Arri Priimägi for being positive, helpful, supportive and energetic; to Esa Räikkönen for interesting discussion on the Q-switched lasers, being the person whose research field has really been close to mine; to Markus Hautakorpi, old roommate, for analytic thoughts and showing me the theorist perspective; to Andriy Shevchenko, the creative scientist and to Jaana Vapaavuori for bringing enthusiastic and new energy to the optics research.

The warmest of my gratitude goes to my parents and sister with her family for the great and reliable support and to my dear friends that have provided me wonderful and relaxing moments during the years.

Espoo, September 2009

Ossi Kimmelma

List of Publications

List of Publications included in the thesis

This thesis consists of an overview and of the following Publications which are referred to in the text by their Roman numerals.

I O. Kimmelma, M. Kaivola, I. Tittonen, and S. C. Buchter "Short pulse, high peak power, diode pumped, passively Q-switched 946 nm Nd:YAG laser", Optics Communications **273** 496-499 (2007).

II O. Kimmelma, I. Tittonen, and S. C. Buchter "Short pulse, diode pumped, passively Q-switched Nd:YAG laser at 946 nm quadrupled for UV production", Journal of European Optics Society: Rapid Publications **03** 08008 (2008).

III O. Kimmelma, I. Tittonen, and S. C. Buchter "Thermal tuning of laser pulse parameters in passively Q-switched Nd:YAG lasers", Applied Optics **47** 4262-4266 (2008).

IV O. Kimmelma and I. Tittonen "Passively Q-switched Nd:YAG pumped UV lasers at 280 and 374 nm", Optics Communications **282** 2930-2933 (2009).

V E. Räikkönen, O. Kimmelma, M. Kaivola, and S. C. Buchter "Passively Q-switched Nd:YAG/KTA laser at 561 nm", Optics Communications **281** 4088-4091 (2008).

Author's contribution

The scientific results presented in this thesis have been carried out at the Department of Micro and Nanosciences during the years of 2005-2009 in Helsinki University of Technology.

The author has written the manuscripts, designed and constructed the setups and performed the measurements in Publications I-IV. In Publication V the author contributed in writing and experiments especially concerning the second harmonic generation.

Abbreviations

BBO	beta-barium borate
BIBO	bismuth triborate
CLBO	cesium lithium borate
DMM	digital multimeter
FWHM	full width at half maximum
IR	infrared
KTA	potassium titanyl arsenate
KTP	kalium titanyl phosphate
LIDAR	light detection and ranging
LBO	lithium triborate
LN	lithium niobate
QPM	quasi-phase-mathing
SESAM	semiconductor saturable absorber mirror
SHG	second harmonic generation
SRS	stimulated Raman scattering
UV	ultra violet
YAG	yttrium aluminium garnet

Contents

1 Introduction

Theoretical predictions for a laser were done as early as in 1917 by Einstein [1]. In thermal equilibrium the key concept of the laser stimulated emission was undetectable and therefore the phenomenon was more or less theoretical. The essential building blocks of a laser did exist, but in various fields of science: stimulated emission was a familiar phenomenon in radio spectroscopy and feedback coupling of oscillators as well as resonator structures in radio engineering. Essential steps towards the laser were the realization of a resonator in the optical range and the insight of making laser material an active medium with gain [2]. This was independently suggested by Basov and Prochorov in 1958 when they introduced the concept of optical pumping. They suggested lifting up the energy of active ions to a higher state by means of light. This is required in order for the stimulated emission to overcome the absorption and the material to build up gain. They received the Nobel prize in 1964 together with Charles H. Townes for their research leading to the demonstration of a laser [3]. It took until 1960 for T. Maiman to report the first laser realized in a Ruby crystal [4]. Since then laser physics has been developing fast with the progress in the fields like optoelectronics and materials science. Lasers have been developed to cover applications in communications, industry, medicine, defence, entertainment, sports, research etc.

As soon as lasers made it possible to produce optical fields with high intensity, the material response to these intense fields showed new and interesting phenomena [5]. Transitions including interaction of many quanta became possible and the material response was extended from linear to nonlinear region. The field of nonlinear optics has the means for versatile

production of laser light at different wavelengths.

Lasers can be pulsed by modulating the losses inside the laser cavity. This can be done by changing the laser cavity alignment or otherwise modulating the losses. In active Q-switching, external signal is used to achieve the pulsing. Typical pulsing methods include mechanical devices or the use of electro or acousto-optic means for loss modulation. In passive Q-switching a saturable absorber is used for modulating losses. When the losses are high, the population inversion builds up and is suddenly released as the losses are saturated creating a powerful pulse. Pulsing leads to high intensity of the laser when compared to a laser running in a continuous wave mode. The high peak power pulses can be used for creating intensities adequate for decent nonlinear conversion. In this thesis this method of creating light pulses at visible and UV-wavelength ranges is used. In a commonly used saturable absorber material of Cr:YAG, a spectral transition is bleached causing drop of absorption. Also semiconductor saturable absorber mirrors (SESAM) can be used to Q-switch or modelock a laser [6]. However, Q-switching using a SESAM is complex since it has to be customized separately for every wavelength.

Pulsed lasers are used in applications like range finding [7, 8], marking, cutting or welding and time resolved spectroscopy [9]. IR-pulses can be used for range finding due to the low absorption and scattering losses in air. Visible laser sources can be used e.g. in projectors. Pulsed lasers at the UV-range can be used in bioanalysis for fluorescence spectroscopy [10–12] giving information also on the dynamics of the system. With deep-UV excitation the study of resonant Raman spectroscopy is possible without overlapping Raman and fluorescence wavelength bands [13]. Furthermore, UV-lasers can be used in micromachining [14] due to the high UV-absorbtion in most materials and for excitation in life time measurements e.g. to examine semiconductor quantum well structures emitting in blue and near UV spectral ranges [15]. Q-switched lasers are used also in tattoo removal for breaking the pigment either by photothermal or photochemical effect [16, 17].

2

Interaction between light and matter in lasing

This thesis explores the research of novel passively Q-switch solid state lasers. Description of the essential effects and parameters that describe a laser are introduced in Section 2.1 together with the laser level schemes and their effect on the lasers in Section 2.2. A laser beam has typically nearly Gaussian intensity distribution. Properties and propagation of Gaussian beams are presented in Section 2.3 together with the description of the beam quality factor. Two important parameters in practical lasers are the threshold and slope efficiency which are covered in Section 2.4. Finally in Section 2.5, the principle of passive Q-switching is presented. This is the method that is used to pulse all of the lasers in this thesis.

2.1 Laser concept

In a process of stimulated emission, a photon evokes emission of another photon by causing an electronic transition. The initial and the triggered photons have the same frequency and phase. This process leads to amplification and depends on the material parameters, amount of excitation on the higher laser level and the photon flux that stimulate the emission. Usually the material gain is not enough to provide gain for a laser and the required extra gain is obtained from an optical resonator. These components are depicted in Figure 2.1a. The optical resonator effectively lengthens the gain medium [18]. The geometry of the resonator has an essential influence on the properties of the laser beam. For a constructive interfer-

ence and gain in the resonator, the optical length of the resonator (l_{opt}) has to be a multiple of half of the wavelength (λ) that is resonating,

$$l_{\mathrm{opt}} = n\frac{\lambda}{2}, \qquad n \in \mathbb{N}. \tag{2.1}$$

In order to get some of the laser light out of the resonator, at least one of the mirrors, the output coupler, has to let some laser light through. Gains of an electronic transition with the width of 120 GHz and resonator with optical length of 10 mm as a function of wavelength are presented in Figure 2.1b.

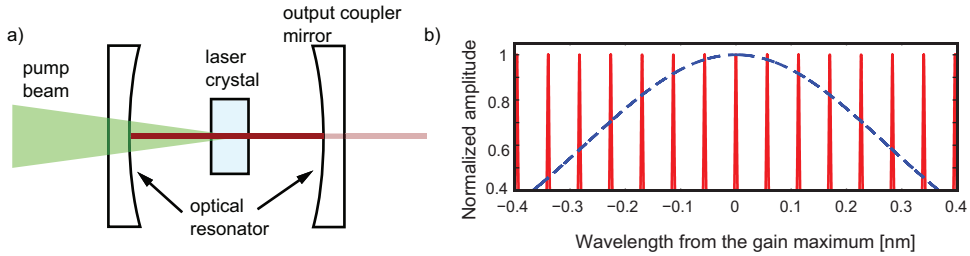

Figure 2.1. a) A schematic picture of a laser gain material with optical pumping inside an optical resonator and b) Nd:YAG gain with the width of 120 GHz (dashed) and resonator gain spectrum(solid) for a 1064 nm laser with the optical length of 10 mm.

2.1.1 Gain media and pumping

Widely used active laser media include gases, dyes, semiconductors, solid state crystals and amorphous glasses. Here we concentrate on solid state materials since solid crystals were used as a laser medium in this thesis.

The term solid state laser usually refers to a dielectric transparent host crystal or glass doped with active ions. Typically glasses have much lower melting temperatures being therefore easier to fabricate even in large size. However, glasses have inferior thermo-mechanical and thermo-optical properties. In amorphous media the spectral gain and absorption lines are broader with lower peak values compared to respective values with crystalline hosts due to inhomogeneous material.[19]

The purpose of pumping in lasers is to achieve population inversion in the laser medium in order to create gain for the laser transition. The gain

coefficient g for the stimulated emission can be calculated as

$$g = \sigma(N_2 - N_1), \tag{2.2}$$

where N_1 and N_2 are the populations for lower and higher laser levels, respectively, and σ is the stimulated emission cross section for the particular transition. Pumping is usually performed via transition which takes population to a level from which the electrons are quickly relaxed down to the higher laser level. Pumping has also been realized directly to the higher laser level [20, 21]. Since the laser transition lifetime is typically and preferably long, the absorbance line width is narrow requiring a pump source with a narrow spectral line width. Pumping through a transition that has a broad absorption line makes pumping efficient even with relatively low quality pump sources. A reasonable pump beam size is further discussed in Section 2.4 but it is typically comparable to the size of the laser mode. The beam quality of the pump source is more critical in lasers operating on low gain transitions and having a short cavity such as described in Publications I,II,IV and V due to the combination of low gain and small laser mode size.

The lasing wavelengths are chosen by the gain of the particular laser transitions and the gain provided by the laser resonator. The relative gain of different transitions of the laser medium is determined by the stimulated emission cross section which depends on the wavelength. However, it is possible to strongly affect the laser resonator gain with the help of coatings. In this way, it is possible to choose the desired laser transition. Long lifetime of the higher laser level helps in building up the population inversion and thus also in reduction of the laser threshold together with the minimization of losses in the resonator.

The ratio between the energies of the laser photon and the pump photon is called quantum efficiency. The difference of these energies is the amount of energy that is lost in the laser crystal for every created photon. Most often this energy is dissipated as heat. Therefore, such properties of the host crystal as thermal conductivity, expansion, tensile strength and temperature dependence of the refractive index are important in laser power scaling. Further losses may be caused by such mechanisms as upconversion which is further discussed in Section 2.1.2. Distribution of the generated heat is affected by the active ion doping concentration

which is a trade off between high absorption and thermal effects. The local heat that is generated causes end-face curvature of the heated laser rod, temperature-dependent variation of the refractive index and stress-dependent variation of the refractive index that shape the incoming beam. The resulting effect of these factors is called thermal lensing. In the case of end pumped laser, the effective focal length caused by the thermal lens can be calculated as

$$f = \frac{\pi K_c w_p^2}{P_H(\mathrm{d}n/\mathrm{d}T)}\Big[\frac{1}{1-\exp(-\alpha l_c)}\Big], \tag{2.3}$$

where K_c is the thermal conductivity of the laser material, $\mathrm{d}n/\mathrm{d}T$ the change of refractive index with temperature, P_H the power that is dissipated in the crystal as heat, w_p pump beam radius, α the absorption coefficient at the pump wavelength and l_c the length of the crystal[22].

The thermal properties of some commonly used laser crystal hosts are presented in Table 2.1.

Table 2.1. Some mechanical and thermal properties of some commonly used laser host crystals. For other than cubic crystals, axis are marked with a and c.[23]

Laser crystal	YAG	YLF	YVO
Thermal expansion	7.5	a 13.0	a 3.1
$[\mathrm{K}^{-1}10^{-6}]$		c 8.0	c 11.4[24]
Thermal conductivity	14	6	5.1[25]
$[\mathrm{W}/(\mathrm{m\ K})]$			
$\mathrm{d}n/\mathrm{d}T$ $[\mathrm{K}^{-1}10^{-6}]$	7.3	π -4.3[26]	c 3.0[24]
		σ -2.0[26]	

2.1.2 Losses

Losses in the laser resonator may originate from absorption, scattering or diffraction. Losses from coatings of the mirrors and crystals can be tailored to be suitable for the specific laser. Other mechanisms that can cause losses are upconversion processes where electron is excited from the upper laser

level after which the electron relaxes back to the higher laser level generating heat. This situation is relevant in lasers that have high inversion density such as many quasi-three level lasers or Q-switched lasers that build up high inversion before the laser threshold is reached. In Auger recombination one of two electrons at the higher laser level transfers its energy to another electron at the same energy level and drops to the ground state. The other electron which receives the energy, is excited to a higher energy level and relaxes down to the higher laser level likely via multiphonon emission producing heat. In summary the process induces absorption and generates heat into the laser crystal [27].

Losses are typically treated as logarithmic losses γ. Logarithmic output coupling loss of a laser resonator $\gamma_{1,2}$ due to mirror transmission $T_{1,2}$, other single pass cavity losses γ_s and total single pass losses γ can be written in the form

$$\gamma_{1,2} = -\ln(1 - T_{1,2}) \ , \ \gamma_s = -\ln(1 - L_s) \ \text{ and } \ \gamma = \gamma_s + \left[\frac{\gamma_1 + \gamma_2}{2}\right], \quad (2.4)$$

where L_s describes single pass losses in the cavity apart from coupling losses.

2.2 Level schemes in lasers

Laser transition for the case of solid state lasers, is a transition between two electronic energy levels in an active laser ion. An incident photon with the energy equal to this transition energy difference can generate stimulated emission. Usually active ions are excited to the upper laser level via a higher energy level that has a significant absorbance and ions decay to the higher laser level. Lasers can be divided to different categories according to the type of the lower laser level.

2.2.1 Three and four-level lasers

In a four-level laser the lower laser level is clearly higher in energy than the ground state and therefore it is not thermally populated. The population inversion is thus easily achieved. Four-level laser is the most used laser scheme in practise. The quantum efficiency is worse than in the other laser

types. The lasers in Publications III-V use four-level laser configuration in a Nd:YAG crystal at 1064 nm and 1123 nm.

In a three-level laser, the lower laser level is the ground state. For such a laser it is hard to achieve population inversion since there is strong population in the lower laser level and therefore the laser threshold is high. On the other hand, the quantum efficiency for a three-level laser is usually good. Surprisingly, the first laser that was realized with a ruby crystal by Maiman was a three-level laser [4].

2.2.2 Quasi-three-level lasers

For a quasi-three-level laser the lower laser level is a sublevel of the ground state. The quantum efficiency is typically quite good due to the low relaxation energy from the lower laser level to the ground level. The lower laser level has nonzero population in the thermal equilibrium which lifts the needed upper laser level population leading to population inversion and thus the laser threshold is increased. The energy level schemes for a quasi-three level and four-level lasers are presented in Figure 2.2.

As Einstein stated roughly one hundred years ago, the cross sections for a nondegenerate system for emission and absorption are the same[1]. For a quasi-three level laser the lower laser level has some population at thermal equilibrium. Therefore, for this kind of laser the electron at the lower laser level can also absorb a photon. This effect called reabsorption reduces the available gain of the laser. The fractional population can be calculated from the Boltzmann equation

$$\frac{N_2}{N_1} = \frac{g_2}{g_1} \exp\left(- \frac{(E_2 - E_1)}{kT} \right), \tag{2.5}$$

where k is the Boltzmann constant and g_2 and g_1 are the degeneracies and N_2 and N_1 the populations for energy levels E_2 and E_1, respectively. The lasers in Publications I and II make use of the quasi-three-level laser transition of Nd:YAG crystal at 946 nm. Properties of some Nd:YAG laser transitions are presented in Table 2.2. Optical properties of some Nd doped host crystals are presented in Table 2.3.

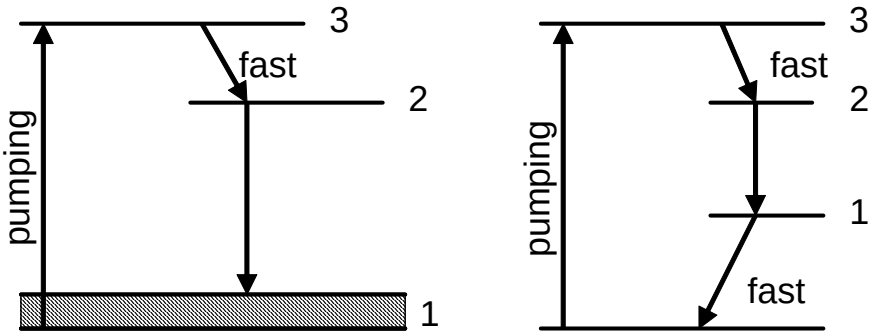

Figure 2.2. Quasi-three-level and four-level laser schemes.

Table 2.2. Properties of Nd:YAG laser transitions: laser wavelength, stimulated emission cross section σ, higher transition level, lower transition level and laser type.

Wavelength [nm]	σ 10^{-20} cm^2	higher level	lower level	laser type
946	5.1[28]	$^4F_{3/2}$	$^4I_{9/2}$	quasi-three
1064	28[23]	$^4F_{3/2}$	$^4I_{11/2}$	four
1123	3.0[28]	$^4F_{3/2}$	$^4I_{11/2}$	four
1318	8.7[28]	$^4F_{3/2}$	$^4I_{13/2}$	four
1338	9.2[28]	$^4F_{3/2}$	$^4I_{13/2}$	four

2.2.3 Rate-equations

Laser behavior can be described with the help of coupled differential equations called rate equations. These equations contain typically many approximations on the laser performance and can not provide accurate quantitative information on the laser. They can still provide valuable qualitative information. The following equations are written for a space independent model with only one laser mode. Let 0 refer to the ground level, 1 to the lower laser level, 2 to the higher laser level and 3 to the level where the electrons are pumped. The relaxations from 1 to 0 and 3 to 2 are assumed to be very fast. The equation for the population at the higher laser level can be written as

$$\frac{dN_2}{dt} = R_p - B\phi N_2 - \frac{N_2}{\tau}, \tag{2.6}$$

Table 2.3. Optical properties for different laser host crystals doped with Nd [23].

Chemical formula	$Y_3Al_5O_{12}$	$LiYF_4$	YVO_4
Abbreviation	YAG	YLF	YVO
Fluorescence lifetime ${}^4F_{3/2}$ [μs]	230[19]	480	98
Refractive index (1064 nm)	1.82	n_o 1.45	n_o 1.96[19]
		n_e 1.47	n_e 2.17[19]
Stimulated emission cross section	2.8[19]	1.8(π)	7.6[19]
${}^4F_{3/2} \rightarrow {}^4 I_{11/2}[10^{-19}\ \mathrm{cm}^2]$		1.2(σ)	
Wavelength ${}^4F_{3/2} \rightarrow {}^4 I_{11/2}$ [nm]	1064	1047(π)	1064
		1053(σ)	
Pump wavelength [nm]	808	792	808
Linewidth FWHM [nm]	0.51[19]	1.44[19]	1.28[19]

where R_p is the pump rate, B the Einstein coefficient and τ the lifetime for the upper laser level. The second term on the right hand side accounts for the loss of population because of stimulated emission and the third one losses due to the spontaneous emission. The relation between Einstein coefficient B and the stimulated emission cross section σ is:

$$B = \frac{\sigma l_c c}{V_a l_{\mathrm{opt}}}, \tag{2.7}$$

where V_a is the volume of the mode in the active medium and l_{opt} the optical length of the resonator.

Rate equation for the number of photons in the cavity ϕ is

$$\frac{d\phi}{dt} = \left(BV_a N_2 - \frac{1}{\tau_c}\right)\phi, \tag{2.8}$$

where

$$\tau_c = \frac{l_{\mathrm{opt}}}{\gamma c} \tag{2.9}$$

is the cavity photon lifetime and γ the logarithmic losses of the cavity.[19]

2.3 Gaussian beam propagation

The laser intensity transversal beam profile that is mainly defined by the optical resonator is typically Gaussian. In this section some properties and propagation of the Gaussian beams are presented. Also the description and measurement of the beam quality factor is explored.

The Gaussian beam intensity profile is of the form

$$I = I_0 \exp(-2x^2/w_x^2) = I_0 \exp(-x^2/2\sigma_x^2), \tag{2.10}$$

where σ_x is the variance of the beam intensity profile and w_x the beam radius from the point $I = I_0/e^2$. This profile can be written with the help of the q-parameter in the form

$$E \propto \exp\left(-jk\Big[z + \Big(\frac{x^2+y^2}{2q}\Big)\Big]\right), \tag{2.11}$$

where x and y are the transversal distances, j the imaginary unit, k is the wavenumber $2\pi/\lambda$ and z is the direction of the beam propagation. The q-parameter is defined as

$$\frac{1}{q} = \frac{1}{R_c} - j\frac{\lambda}{\pi w^2}. \tag{2.12}$$

The q-parameter describes the beam with two real parameters: beam $1/e^2$ radius w and radius of curvature (ROC) R_c. Other widely used way to describe the beam width is full width at half maximum (FWHM) beam diameter. The ratio of the FWHM beam width and $1/e^2$ beam radius for a Gaussian beam is

$$1.18 \times w_{1/e^2} = w_{\mathrm{FWHM}}. \tag{2.13}$$

In the direction normal to the propagation direction, the beam can be described in polar coordinates in a form

$$E = E_0 e^{-\frac{r^2}{w^2}}, \tag{2.14}$$

where r is the distance from the center point of the beam. At the point $r = w$ the field gets the value $E = E_0/e$. The beam radius parameter hereby describes the width of the Gaussian beam. It can be shown that

the ray transfer matrix or ABCD matrix applies also for Gaussian beams [19, 29]:

$$q_1 = \frac{Aq_0 + B}{Cq_0 + D} \tag{2.15}$$

The matrix for describing the propagation of the beam in free space with the length of l in the medium with refractive index n is [19]

$$M_L = \begin{pmatrix} 1 & l/n \\ 0 & 1 \end{pmatrix}. \tag{2.16}$$

The effect of a mirror with radius of curvature R_{curv} is given by

$$M_R = \begin{pmatrix} 1 & 0 \\ -2/R_{\mathrm{curv}} & 1 \end{pmatrix}, \tag{2.17}$$

and that of a lens with the focal length of f:

$$M_{\mathrm{lens}} = \begin{pmatrix} 1 & 0 \\ -1/f & 1 \end{pmatrix}. \tag{2.18}$$

Thermal lens is also formed inside the laser crystal in longitudinal pumping as discussed in Section 2.1.1. With these matrices it is possible to model the propagation of Gaussian beams through complex optical systems and resonators as discussed in Section 2.3.2.

2.3.1 M^2 factor

For the diffraction limited beam the product of beam divergence angle θ_{dl} and the size of the beam waist w_{dl} is constant λ/π. The M^2 parameter describes the quality of the beam and is the ratio of this product for the beam of interest to the diffraction limited beam. It can be calculated as

$$M^2 = \frac{\theta_{\mathrm{m}} w_{\mathrm{m}}}{\theta_{\mathrm{dl}} w_{\mathrm{dl}}} = \theta_{\mathrm{m}} w_{\mathrm{m}} \pi/\lambda, \tag{2.19}$$

where θ_{m} is the measured divergence angle and w_{m} the $1/e^2$ radius determined from the intensity profile for the beam of interest.

For nondiffraction limited beams, the effect of the M^2 parameter in the Gaussian beam propagation calculations can be taken into account by writing the wavelength λ in a form

$$\lambda = M^2 \lambda_0, \tag{2.20}$$

where λ_0 is the actual wavelength of the laser beam [30].

Beam width for an arbitrary beam can be defined by using the second moment. The second moment of the intensity profile $I(x, y)$ across the rectangular coordinate x can be calculated as

$$\sigma_x^2 = \frac{\iint (x - x_0)^2 I(x, y) \mathrm{d}x\mathrm{d}y}{\iint I(x, y) \mathrm{d}x\mathrm{d}y}, \tag{2.21}$$

where x_0 is the center of gravity of the beam. The relation of the variance and the beam waist for the Gaussian intensity profile of the form of Eq. 2.10 is $w_x = 2\sigma_x$ [31]. The beam width w is also adopted to describe nearly Gaussian beam profiles in this thesis.

Measurement results for calculation of M^2 values for the 374-nm laser in Publication IV are presented in the following graphs. Intensity profiles of the beam at different distances from the waist are presented in Figure 2.3. Cross sections at the center of gravity point for the beams at the walk-off and nonwalk-off directions are plotted in Figures 2.4 and 2.5, respectively. The FWHM beam widths by the second moment method calculated from the data presented in Figure 2.3 using Equation 2.21 are presented in Figures 2.6 and 2.7 together with Gaussian fits for nonwalk-off and walk-off directions, respectively. Obtained M^2 values for the nonwalk-off and walk-off directions are 1.3 and 1.7, respectively.

2.3.2 Laser cavity design

For a stable optical resonator, the Gaussian beam propagates so that the beam parameters do not change after a roundtrip in the resonator. This can be written using ray transfer matrix formalism with r being the distance from the optic axis and r' the angle between the ray propagation direction and the optic axis [32]

$$\begin{pmatrix} r_N \\ r'_N \end{pmatrix} = \begin{pmatrix} A & B \\ C & D \end{pmatrix}^N \begin{pmatrix} r_i \\ r'_i \end{pmatrix}. \tag{2.22}$$

In order to r_N stay finite when $N \to \infty$ we get the requirement

$$BA - CD = 1. \tag{2.23}$$

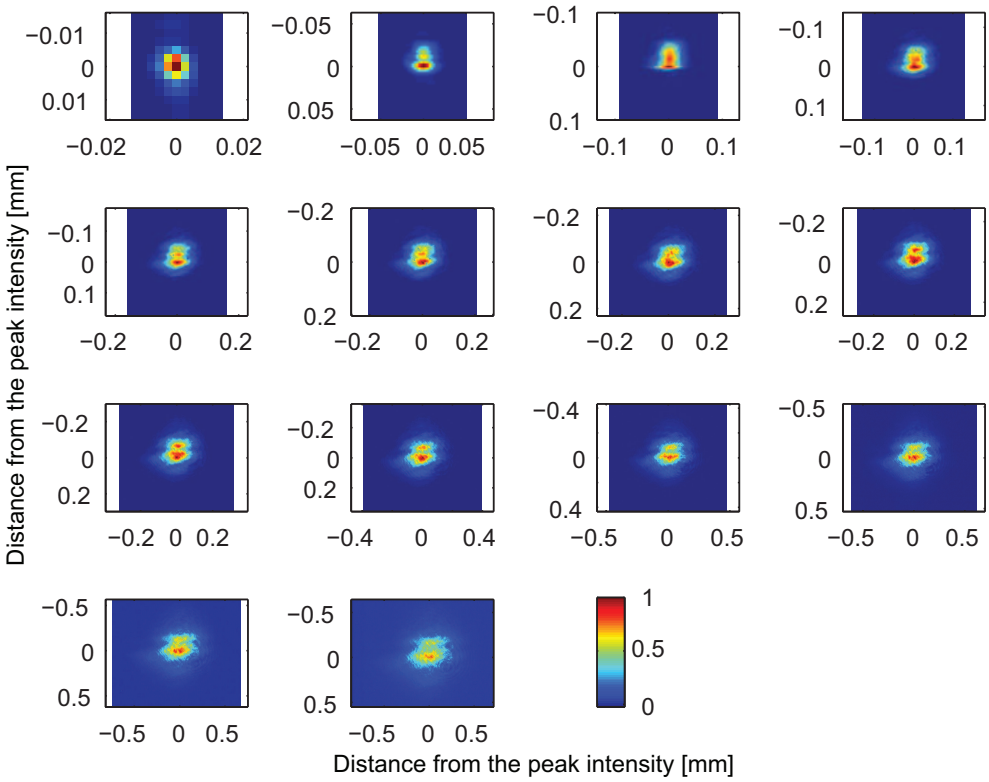

Figure 2.3. Images of the beam at different distances from the waist. Respective cross sections and beam widths are presented in Figures 2.4, 2.5, 2.6 and 2.7.

Unchanged Gaussian beam after one roundtrip in the resonator and the ABCD-law Eq. 2.15 leads to the condition

$$q = \frac{Aq + B}{Cq + D} \tag{2.24}$$

The q-parameter is complex for a real beam. When solving for q, this leads to the requirement for the discriminant

$$(D - A)^2 + 4BC < 0. \tag{2.25}$$

When Eq. 2.23 is substituted, we get the stability requirement

$$(D + A)^2 < 4 \text{ or } -1 < \frac{A + D}{2} < 1 \tag{2.26}$$

The ABCD matrix for a resonator with two mirrors with radii R_1 and R_2 separated by the length l, gets the form

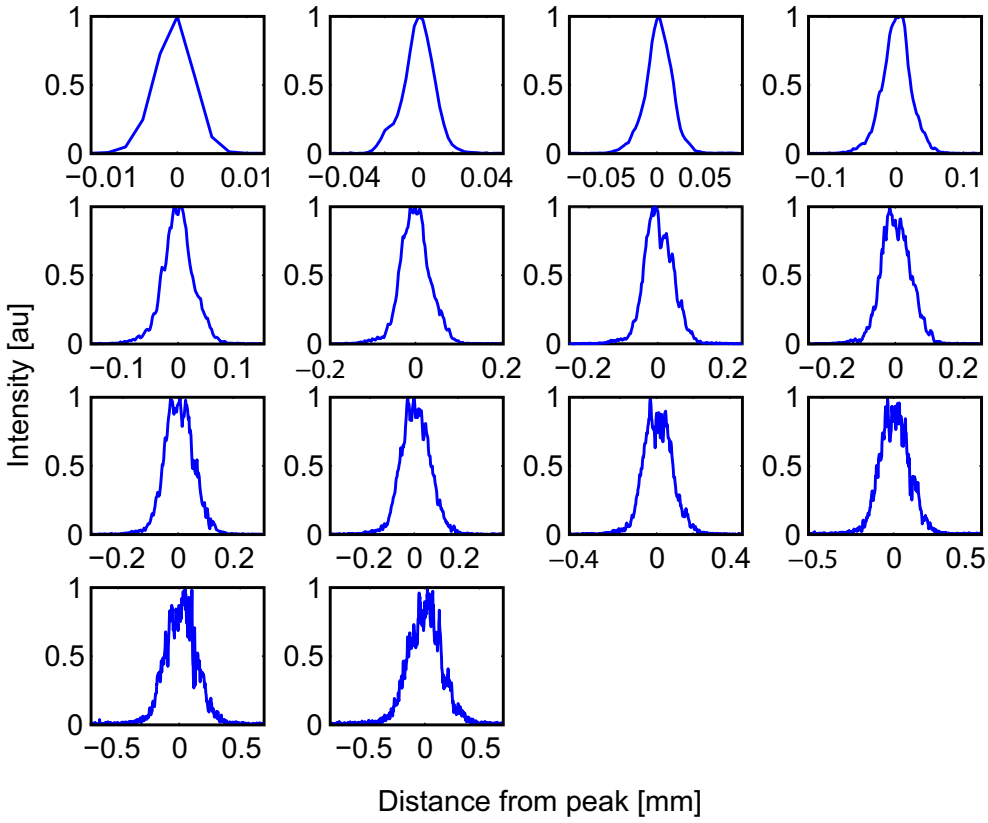

Figure 2.4. Cross section of the 374 nm laser intensity profile at the center of gravity point in a direction with no walk-off. Respective beam widths and measurement distances from the focus are presented in Figure 2.6.

$$\begin{pmatrix} A & B \\ C & D \end{pmatrix} = \begin{pmatrix} 1 & 0 \\ -2/R_1 & 1 \end{pmatrix} \begin{pmatrix} 1 & l \\ 0 & 1 \end{pmatrix} \begin{pmatrix} 1 & 0 \\ -2/R_2 & 1 \end{pmatrix} \begin{pmatrix} 1 & l \\ 0 & 1 \end{pmatrix} \tag{2.27}$$

$$= \begin{pmatrix} 1-2\frac{l}{R_2} & 2l-2\frac{l^2}{R_2} \\ -\frac{2}{R_1}-\frac{2}{R_2}+4\frac{l}{R_1R_2} & 1-2\frac{l}{R_2}-4\frac{l}{R_1}+4\frac{l^2}{R_1R_2} \end{pmatrix} \tag{2.28}$$

From this matrix the stability condition Eq. 2.23 gets the form

$$-1 < 1 - \frac{2l}{R_1} - \frac{2l}{R_2} - 2\frac{l^2}{R_1R_2} < 1. \tag{2.29}$$

The same equation written with the help of parameters $g_1 = 1 - l/R_1$ and $g_2 = 1 - l/R_2$ simplifies to

$$0 < g_1 g_2 < 1. \tag{2.30}$$

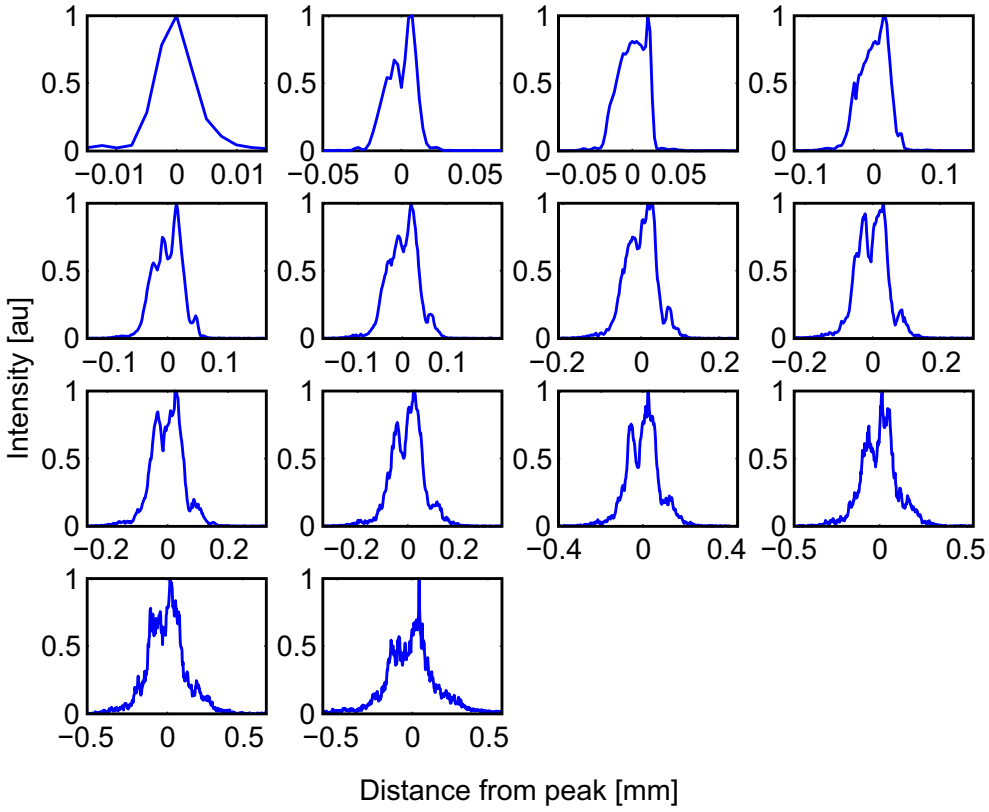

Figure 2.5. Cross section of the 374 nm laser intensity profile at the center of gravity point in a direction of the walk-off. Respective beam widths and measurement distances from the focus are presented in Figure 2.7.

The width of the beam waist in the resonator can be calculated with the help of Eq. 2.24 and noting that the q value gets purely imaginary value (from Eq. 2.12) at the waist since radius of curvature $R_c \to \infty$. With the help of g parameters the waist value gets the form

$$w_0 = \left(\frac{l\lambda}{\pi}\right)^{1/2} \left[\frac{g_1 g_2 (1 - g_1 g_2)}{(g_1 + g_2 - 2 g_1 g_2)^2}\right]^{1/4} \tag{2.31}$$

and especially for a plano-convex resonator which is the resonator type used in this thesis[19]

$$w_{0\mathrm{pc}} = \sqrt{\frac{l\lambda}{\pi}} \left(\frac{g}{1-g}\right)^{\frac{1}{4}}. \tag{2.32}$$

The FWHM waist diameter as a function of the cavity optical length for a resonator that is used in Publications I-II is shown in Figure 2.8. The

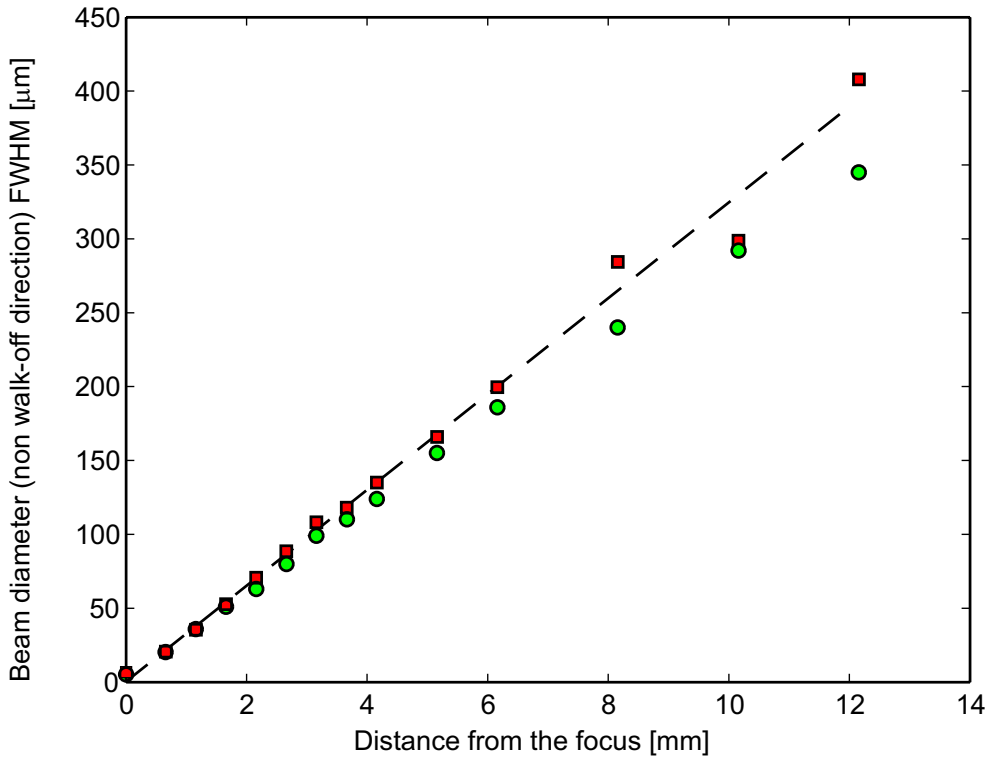

Figure 2.6. FWHM width for the 374 nm laser beam (Publication IV) as a function of the distance from the beam waist for nonwalk-off direction. Beam widths using the method of second moment are plotted as squares and the Gaussian fits to the intensity profiles as circles. Dashed line is the fit to the second moment method results. The divergence angle of this line resulted in the M^2 value of 1.3.

resonator comprises of a plane mirror and a mirror with the radius of curvature of 150 mm.

The laser resonator mode size depends also on more dynamic effects in addition to the cold cavity mode size. The pumping laser affects the mode size as does the saturable absorber in passively Q-switched lasers. The related effects are thermal lensing that was discussed in Section 2.1.1, aperture guiding [33] and gain guiding [34]. Aperture guiding and gain guiding take into account the spatial gain and absorption in the laser crystal. Absorption profile that depends on longitudinal pumping of the laser crystal in quasi-three level lasers is caused by the lower laser level population. The pump beam bleaches the lower laser level which reduces the absorption and as a result an aperture is formed [33]. Gain guiding

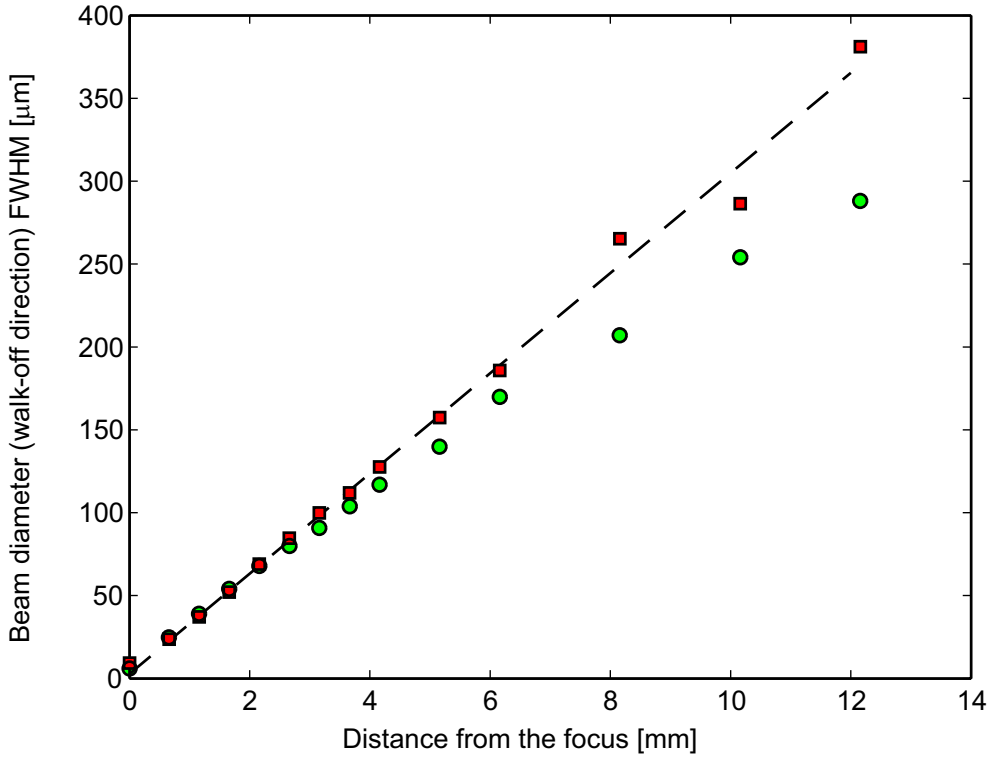

Figure 2.7. FWHM width for the 374 nm laser beam (Publication IV) as a function of the distance from the beam waist for walk-off direction. Beam widths using the method of second moment are plotted as squares and the Gaussian fits to the intensity profiles as circles. Dashed line is the fit to the second moment method results. The divergence angle of this line resulted in the M^2 value of 1.7.

takes into account the spatial profile of the pumping beam [34]. These methods have further been developed to take into account the saturable gain [35] and iterative method to include mode calculations for passively Q-switched lasers discussed in Section 2.5.1 [36]. In passive Q-switching discussed in Section 2.5.1 the laser mode size changes also in time due to the widening of saturated area of the saturable absorber during pulsing [7, 36].

2.4 Laser threshold and slope efficiency

The lasing threshold for a laser with the mirror reflectivities of R_1 and R_2 and active material with length l_c can be calculated from the gain of one

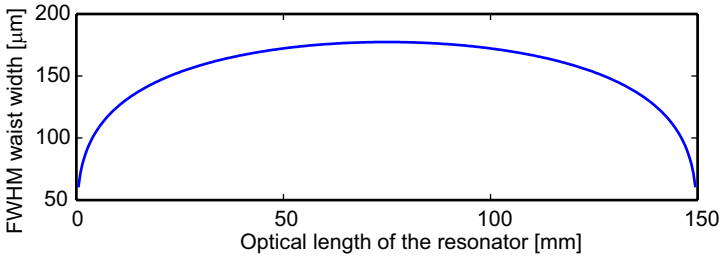

Figure 2.8. FWHM waist diameter as a function of the cavity length. One mirror is a plano mirror and the other one has the radius of curvature of 150 mm.

round trip in the resonator. The gain coefficient per unit length is g. The intensity gain for one round trip is $\exp(2gl_c)$. Other than mirror losses L_i can be added with a factor of $(1 - L_i)^2$. The threshold gain for one round trip can be calculated from

$$R_1 R_2 (1 - L_i)^2 e^{2gl_c} = 1. \tag{2.33}$$

When the gain is larger than one, the radiation at the proper frequency builds up fast until it depletes the upper level and reduces the value of g. The loss mechanisms include reflection, scattering, diffraction and absorption losses in the mirrors and in the amplifying medium.

The threshold pump power can be derived from the rate equation for the population at the higher laser level Eq.2.6. The pump rate needed to overcome the number of atoms decaying spontaneously is $R_p = N_2/\tau$, where N_2 is the population of the upper laser level and τ is the effective life time of the upper laser level. By calculating the overlap integrals between the pump beam and laser cavity modes for longitudinal Gaussian pumping, the absorbed threshold pumping power gets the form

$$P_{\mathrm{a,th}} = \frac{\pi h \nu_p}{2\sigma_e \eta_p \tau}(w_0^2 + w_p^2)\left(\frac{\gamma_e}{2} + \gamma_i l_c + \sigma f_a N_0 l_c\right), \tag{2.34}$$

where γ_i represents the intrinsic losses in the gain medium such as scattering or impurity absorption, γ_e includes the extrinsic losses such as output coupling not dependent on the gain medium, ν_p is the pump frequency, σ_e is the effective stimulated emission cross section, η_p is the pump quantum efficiency which is the number of ions in the upper manifold created by each absorbed photon and w_o and w_p are the beam waist radii for

the lasing mode and pump mode respectively. One can notice that threshold is inversely proportional to the stimulated emission cross section σ_e and higher laser level life time τ. The factor $\sigma f_a N_0 l_c$ includes the possible extra inversion needed to overcome the population at lower laser level where σf_a is the effective absorption cross section for lower laser level, f_a the fractional occupation of the lower laser level and N_0 the dopant concentration. The value of f_a for 946 nm Nd:YAG transition is 0.0074. The incoming power P_{i} that is needed to achieve the absorbed power $P_{\mathrm{a,th}}$ is

$$P_{\mathrm{i,th}} = \frac{P_{\mathrm{a,th}}}{1 - \exp(-\alpha l_c)}, \tag{2.35}$$

where α is the absorbtion coefficient of the laser crystal for the pump wavelength.[37, 38]

Reabsorption increases the threshold pump power. According to Equation 2.34, the laser threshold pump power is reduced by minimizing the laser- and pump waist radii w_l and w_p. The analysis did not take into account the diffraction of the pump beam or the laser mode within the laser medium. The mode overlap is affected by the pump beam quality which can be represented by the M^2 parameter. The diffraction and pump beam quality can be taken into account by taking the average or root mean square radii of the pump and laser modes and using the former analysis for these averaged values [39]. These average values are then used to optimize the actual waist radii. The average value of the given beam waist radius w_0 at one end of the crystal is given by

$$\bar{w}^2 = w_0^2 + \frac{1}{3}\left(\frac{M^2 \lambda l_c}{\pi n w_o}\right)^2. \tag{2.36}$$

By differentiating Equation 2.36, the optimum value for w_0 can be found by finding the minimum value for $\bar{w}$

$$w_{0,\mathrm{opt}} = \left(\frac{1}{\sqrt{3}}\frac{M^2 \lambda l_c}{\pi n}\right)^{1/2}. \tag{2.37}$$

The laser beam is assumed to be diffraction limited. The minimum attainable average mode radius is

$$\bar{w}_{\mathrm{min}} = \left(\frac{2}{\sqrt{3}}\frac{M^2 \lambda l_c}{\pi n}\right)^{1/2} = \sqrt{2} w_{0,\mathrm{opt}}. \tag{2.38}$$

The value $w_{0,\mathrm{opt}}$ is the waist value which results in the smallest available average beam mode size in the crystal and in the optimized beam waist value for the minimized threshold.

Laser slope efficiency is the ratio of the change of the laser power to the change of the absorbed pump power

$$\eta_s = \frac{dP_{\mathrm{out}}}{dP_{\mathrm{p}}}. \tag{2.39}$$

This efficiency can be approximated to consist of three terms

$$\eta_s = \eta_q \eta_c \eta_t, \tag{2.40}$$

where quantum efficiency η_q is the ratio of the laser photon energy to the pump photon energy, the output coupling η_c is the fraction of laser photons coupled out of the cavity and the term η_t takes into account the overlapping of pump and laser transverse modes. If modematching between the pump and laser modes is assumed ($\eta_t \approx 1$)

$$\eta_s = \frac{h\nu}{h\nu_p} \frac{T_2}{L_r}, \tag{2.41}$$

where T_2 is the transmission of the coupling mirror and L_r describes all losses for one roundtrip. [38]

Absorbed threshold power and slope efficiencies as a function of laser crystal mount temperature are presented in Figure 2.9 for a Q-switched 1064 nm laser referred to laser 1 in Publication III. The temperature affects the stimulated emission cross section. One can notice the increase of the threshold power with temperature as is expected from Equation 2.34 and the unchanged slope efficiency as suggested by Equation 2.41 as there is no dependency on the stimulated emission cross section. Theoretical approximation with a small pump beam for the theoretical maximum slope efficiency given by Eq. 2.41 would suggest efficiency of 0.57. Saturated losses for the Q-switch crystal are 2% per pass [V]. The measured average efficiency is 0.33. Theoretical minimum for the laser threshold from Eq. 2.34 gives absorbed power of 130 mW whereas the measured result is 280 mW.

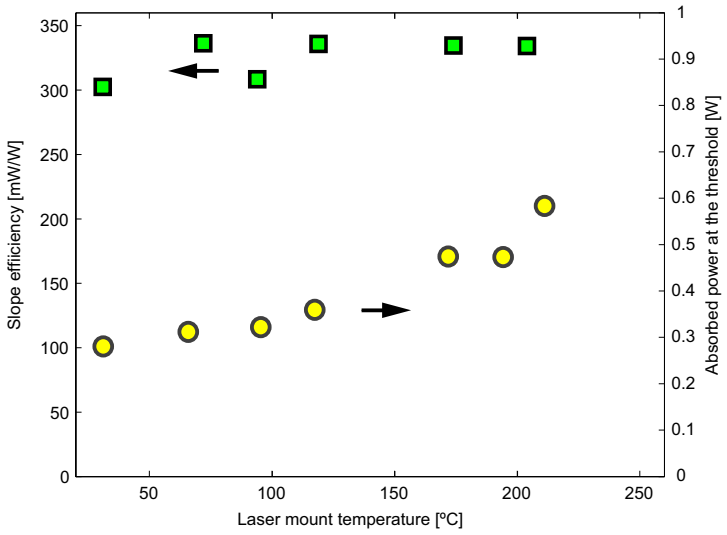

Figure 2.9. Slope efficiency and absorbed laser threshold as a function of the laser crystal mount temperature for laser 1 in Publication III.

2.5 Pulsed mode lasers

With pulsed lasers it is possible to achieve very high intensity even with a simple and small device. Pulsed lasers are used in various applications that require extreme temporal laser intensity like e.g. marking and non-linear conversions. Some applications as tattoo removal or laser cutting require large intensity without too much generated heat. Applications like laser range finding and LIDAR (light detection and ranging) make use of the laser pulse propagation.

Pulsing may be generated by such techniques as Q-switching (active or passive), gain switching or mode locking. Q-switching is explored more thoroughly in the next section. In gain switching, an intense pump pulse exceeding clearly the laser threshold creates a strong population inversion in the gain medium before the lasing starts and a pulse builds up. In other words the first spike of relaxation oscillations is used for the pulse generation. Because of the fast pumping process, also gain media such as titanium-sapphire (Ti:Al_2O_3) crystal with short life time can be used for a gain-switched laser.

In mode locking large amount of longitudinal modes are synchronized

to produce short high peak power pulse typically with the pulse width from the ps to the fs range. Mode locking can be done actively by using external modulation to introduce synchronization of the laser modes or passively by using an element that self-modulates the laser.

2.5.1 Passive Q-switching

Q-switching refers to the fact that the pulses from a laser are formed by altering the Q-value of the resonator which is defined by the ratio of stored energy in the resonator E_{stored} to the lost energy per resonator cycle E_{loss} multiplied by 2π [19],

$$Q = \frac{2\pi E_{\text{stored}}}{E_{\text{loss}}} \tag{2.42}$$

or with the help of oscillating frequency ν_0 and the FWHM resonance width $\Delta\nu$ [23]

$$Q = \frac{\nu_0}{\Delta\nu}. \tag{2.43}$$

There are various ways to affect the Q-value with the help of losses of the resonator. Active methods are electro optical, acousto-optical or mechanical modulation schemes. A passive method is to use a saturable absorber. All experimental work in this thesis is carried out by using chromium doped YAG (Cr:YAG) saturable absorber. It is a material where the absorption is altered by the fluence. The absorber is bleached when high enough fluence goes through the crystal. The bleaching process is based on saturation of a spectral transition. Inside the laser cavity, the loss of a saturable absorber is first high enough to prevent lasing. This makes it possible to reach high inversion by pumping electrons to the upper laser level. The gain builds up with the increase of the upper laser level population until it overcomes the extra loss introduced by the absorber. Finally, the created photons bleach the saturable absorber[40]. A strong pulse is launched until the stimulated emission eats up the population at the higher laser level. The lifetime of the excited state for Cr:YAG is much longer than the laser pulse, in the order of 4 μs while the pulse length is in the order of nanoseconds. Typical time between the pulses in this thesis is in the order of 100 μs. The lifetime measurement result of active ions in Cr:YAG excited by a 1064 nm pulse is presented in Figure 2.10.

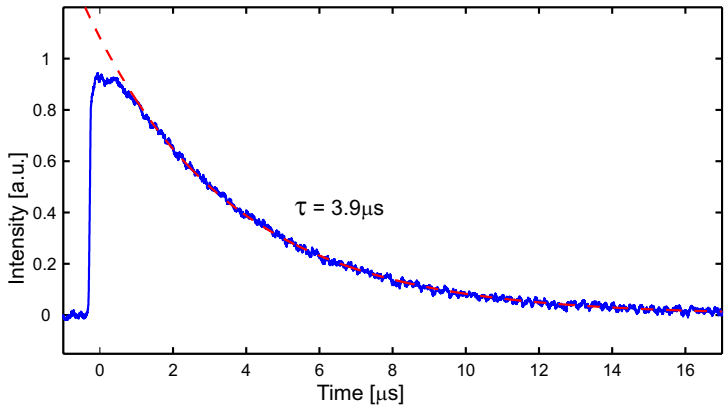

Figure 2.10. Fluorescence lifetime measurement of Cr:YAG crystal at 35°C excited by a 1064 nm laser pulse with exponential fit with lifetime of 3.9μs.

The passive Q-switch structure is very simple and it offers a miniature, robust and low-cost system. The drawbacks of passive Q-switching are the lack of an external trigger, jitter which is the variation of the time between the pulses, the limited loss introduced by the saturable absorber which limits the available pulse build-up time and the residual absorption of the saturated passive Q-switch. Factors affecting to the timing jitter are pump intensity variation, changes in spectral and spatial properties of the pump, and changes of laser spatial modes. Because of these phenomenon, the threshold condition is slightly modified affecting to the pulse build-up time. Reduction of the jitter has been demonstrated with the use of external laser that triggers the pulse by bleaching the Cr:YAG crystal.[41]

The period between the pulses T_{per} can be approximated with the simple formula

$$T_{\mathrm{per}} = \frac{\tau P_{\mathrm{abs,thresh}}}{P_{\mathrm{abs}}}, \tag{2.44}$$

where τ is the spontaneous emission lifetime of the gain medium, P_{abs} is the total amount of the pump power absorbed within the lasing mode volume, and $P_{\mathrm{abs,thresh}}$ the pump power required for reaching the threshold inversion density [42]. Approximation for the laser in Publication IV gives T_{per} of 200 μs while the measured time between the pulses was 150 μs.

The absorbed pump power has only minor effects to the pulse energy and the peak power through effects like aperture guiding, thermal lensing or pump induced bleaching. The Q-switched lasing threshold is reached

when the population inversion density gets the value [23]

$$N = \frac{1}{2\sigma l_{\mathrm{c}}}\left(\ln\frac{1}{R} + L_r\right), \tag{2.45}$$

where σ is the emission cross section at the lasing wavelength, l_{c} the length of the active medium, R the reflection coefficient of the mirror and L_r the roundtrip losses in the cavity (scattering, diffraction, unsaturated losses of the saturable absorber and laser crystal absorption). The threshold increases when having higher losses in the absorption of the Q-switch crystal, in the cavity, in the coupling mirror or with a smaller stimulated emission cross section.

A commonly used saturable absorber material is Cr^{4+}:YAG. It has high damage threshold, high chemical stability and reliability, good thermal conductivity and broad absorbance bandwidth. The simplified four-level model describing the saturable absorption energy levels in Cr^{4+}:YAG is shown in Fig 2.11. The transitions $3 \rightarrow 2$ and $4 \rightarrow 2$ are fast while the transition $2 \rightarrow 1$ is slow. The transitions $1 \rightarrow 3$ and $2 \rightarrow 4$ give rise to absorption at the laser wavelength with the corresponding cross sections of σ_{gs} and σ_{es}, respectively. The absorption saturates as the ground level is bleached and the electrons are lifted to the level 2 via quick relaxation from level 3. The saturated absorption is induced by the excited state absorption from level 2 to 4. Ground and excited state cross sections for different wavelengths are presented in Table 2.4. One should however note that there is a large uncertainty in the cross section values. Reported cross section values vary more than one order of magnitude whereas the ratio σ_{gs}/σ_{es} vary significantly less[43].

Table 2.4. Properties of Cr:YAG at different wavelengths λ: ground state cross section σ_{gs}, exited state cross section σ_{es}, ratio of cross sections $\sigma_{\mathrm{gs}}/\sigma_{\mathrm{es}}$ and lifetime τ [IV][44].

λ	946	1064	1123
σ_{gs} $[10^{-18}\mathrm{cm}^2]$	4[44]	3.2[40]	
σ_{es} $[10^{-18}\mathrm{cm}^2]$	1.1[44]	0.45[40]	
$\sigma_{\mathrm{gs}}/\sigma_{\mathrm{gs}}$	3.6[44]	3.7[V]	5.5[V]

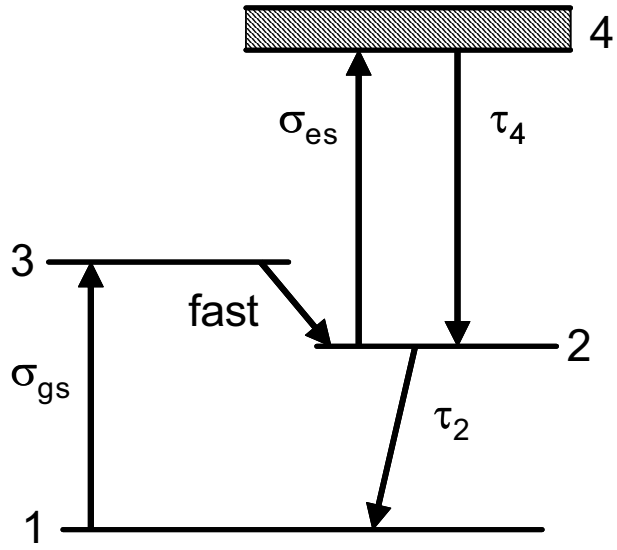

Figure 2.11. A schematic picture of the Cr^{4+}:YAG energy levels.

Expressions for pulse peak power, energy and pulse width have been derived by X. Zhang [45] starting from the rate equations for Q-switching including the excited state absorption:

$$\frac{\mathrm{d}\phi}{\mathrm{d}t} = \frac{\phi}{t_r}\Big[2\sigma n_i l - 2\sigma_{\mathrm{gs}} n_{s1} l_s - 2\sigma_{\mathrm{es}}(n_{s0} - n_{s1}) l_s - \ln\frac{1}{R} - L_r\Big] \tag{2.46}$$

$$\frac{\mathrm{d}n_i}{\mathrm{d}t} = -\gamma\sigma c\phi n_i \tag{2.47}$$

$$\frac{\mathrm{d}n_{s1}}{\mathrm{d}t} = -\sigma_{\mathrm{gs}} c\phi n_{s1}, \tag{2.48}$$

where ϕ is the photon density inside the laser resonator, l_s is the length of the saturable absorber, n_{s1} is the instantaneous population density at the level 1, n_{s0} is the total population density contributing to the transitions during pulsing, n_i is the instantaneous population inversion density, σ is the effective stimulated emission cross section, $t_r = 2l_{\mathrm{opt}}/c$ is the round-trip transit time of light in the resonator of optical length l_{opt}, R is the reflectivity of the output mirror, γ is the inversion reduction factor, and L_r covers the remaining round-trip dissipative optical losses, including the crystal absorption loss of saturable absorber and laser crystal. The inversion reduction factor $\gamma = f_a + f_b$, where f_a and f_b are the Maxwell-Boltzmann probabilities for the upper and lower laser levels, respectively [46].

The developed models typically simplify the Q-switching process and thus give optimistic results for the pulse parameters. A detailed information on spectral parameters like thermalization times, lower laser level lifetimes and emission cross section values for laser crystals and saturable absorption crystals would be needed in order to achieve more exact simulation results and understanding on all of the effects during pulsing[43, 47]. One such effect is secondary or satellite pulsing meaning typically smaller pulses after the main laser pulse. This phenomenon is proposed to be related to a bottleneck effect during the laser pulse[47, 48]. Degnan *et al.* considers that the bottleneck would be the thermalization among the Stark sublevels whereas Ng *et al.* suggests that it would be caused by the finite lifetime of the lower laser level. Bottleneck effect is inversely proportional to the relaxation parameter Γ_x

$$\Gamma_x = \gamma_x t_c, \tag{2.49}$$

where γ_x is the relaxation rate for the specific transition and t_c the resonator photon lifetime

$$t_c = \frac{t_r}{\ln(1/R) + L_r} = \frac{2l_{\text{opt}}}{c(\ln(1/R) + L_r)}, \tag{2.50}$$

where L_r is the resonator round-trip loss and R the output coupling mirror reflectivity[47]. Satellite pulses were observed frequently at the wavelength of 946 nm in Publication II. For this laser, the peak power was optimized to be high so that the relaxation from lower laser level can form a bottleneck to the pulse formation. An example of the time trace of a pulse is presented in Figure 2.12.

The temporal properties of the laser pulse can be divided to two parts: leading edge and trailing edge. The leading edge properties are determined by pulse build up: losses and feedback. The losses consist of the unsaturated losses of the saturable absorber, coupling losses and other dissipative losses. The stimulated emission cross section affects also the pulse build up through the available gain of the laser. The trailing edge of the pulse is to a great extent dictated by the laser cavity properties, in other words, the cavity photon lifetime Eq. 2.50. For a given laser, shortening the cavity length will shorten the pulse due to the shortening of the cavity photon lifetime. Increase of the outcoupling for the laser shortens

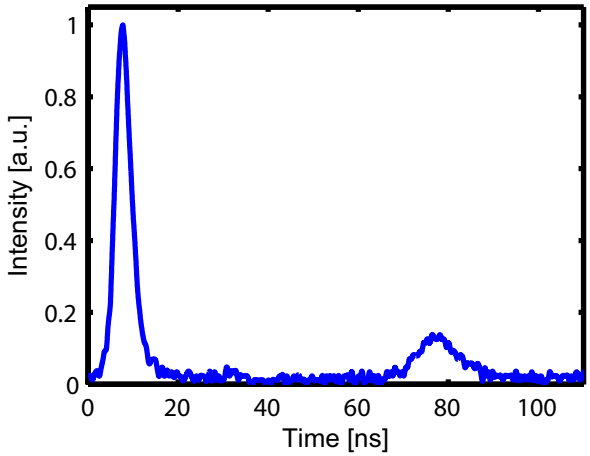

Figure 2.12. A time trace of a single 946 nm laser pulse with a typical after pulse.

also the cavity photon lifetime shortening the trailing edge of the pulse. However, it lengthens at the same time the leading edge of the pulse due to the decelerated pulse buildup so the outcoupling has an optimum in terms of minimizing the pulse length. Increasing the outcoupling also lifts up the laser threshold. The shortest pulse is obtained when the leading and trailing edges are equally long. [49]

If significant part of the pump power goes through the laser crystal, the remaining pump laser power can contribute to bleaching of the Cr:YAG crystal. This effect can be significant especially in lasers that produce short pulses and both the laser crystal and the cavity length are short. Then the remaining pump laser beam has still high intensity at the point where the saturable absorber is located. The effect is called pump induced bleaching and it can reduce the pulse energy and peak power. The intensity of the pump laser at saturable absorber can be minimized by placing the absorber as far from the pump focus as possible as the pump beam diverges typically fast due to the low beam quality. However, this is not possible with lasers having short cavities. The saturation intensity for Cr:YAG is 30 $\mathrm{kWcm^{-2}}$. [50]

A practical limitation of the laser design is the high intensity inside the laser resonator. The damage threshold for the crystals and coatings for crystals or the mirror can restrict the highest peak power that is achievable.

The power inside a Fabry-Perot resonator can be calculated as [46]

$$P_r = P_{\text{out}}\left(\frac{1+R}{1-R}\right), \tag{2.51}$$

where R is the reflectance for the coupling mirror and P_{out} is the power outside the resonator. The coupling mirror is assumed to be highly reflecting. The relation between the maximum intensity and the optical power for a Gaussian beam is [51]

$$P = \frac{1}{2} I_0 \pi w_o^2 \tag{2.52}$$

With the laser presented in Publication I the peak power was 3.8 kW, output coupler mirror had reflectance 92% with 15 cm curvature and the cavity waist radius was approximately 100 μm. The resulting power inside the cavity was 91 kW and the maximum intensity inside the cavity was 580 MW/cm^2. This value can be compared to the damage threshold of 500 MW/cm^2 given by an optics manufacturer Castech for Cr:YAG saturable absorber.

3
Nonlinear optics

With the use of laser light sources, coherent beams with high intensities can be created. Shortly after the demonstration of the laser a new research field of, nonlinear optics, was born in 1961 when the first observations of nonlinear optical phenomena were made[5]. Nonlinear optics is the study of phenomena that occur as a consequence of the modification of the optical properties of a medium by the presence of light [52]. In order to achieve efficient conversion from one wavelength to another, it is necessary to organize a constructive interference to the created new optical component along the nonlinear crystal. This is called phase matching and it is discussed further in the next section.

The polarization that is induced by light with the field strength $\mathbf{E}$ can be expressed as a series

$$\begin{aligned} \mathbf{P} &= \varepsilon_0(\chi^{(1)}\mathbf{E}(t) + \chi^{(2)}\mathbf{E}^2(t) + \chi^{(3)}\mathbf{E}^3(t) + \ldots) \\ &= \mathbf{P^{(1)}}(t) + \mathbf{P^{(2)}}(t) + \mathbf{P^{(3)}}(t) + \ldots. \end{aligned} \tag{3.1}$$

In case the incident optical field consists of two frequency components ω_1 and ω_2 the total field is

$$\mathbf{E}(t) = \mathbf{E}_1 e^{-i\omega_1 t} + \mathbf{E}_2 e^{-i\omega_2 t} + c.c. \tag{3.2}$$

The second-order contribution from Eq. 3.1 to the nonlinear polarization is given by

$$\begin{aligned} \mathbf{P^{(2)}}(t) &= \varepsilon_0\chi^{(2)}\mathbf{E}^2(t) \\ &= \varepsilon_0\chi^{(2)}[\mathbf{E_1}^2 e^{-2i\omega_1 t} + \mathbf{E_2}^2 e^{-2i\omega_2 t} + 2\mathbf{E_1}\mathbf{E_2} e^{-(\omega_1+\omega_2)t} + \\ &\quad 2\mathbf{E_1}\mathbf{E_2^*} e^{-(\omega_1-\omega_2)t} + c.c.] + 2\chi^{(2)}[\mathbf{E_1}\mathbf{E_1^*} + \mathbf{E_2}\mathbf{E_2^*}]. \end{aligned} \tag{3.3}$$

The amplitudes of the different frequency components of the nonlinear polarization are given by

$$\begin{aligned} P(2\omega_1) &= \varepsilon_0 \chi^{(2)} E_1^2 && (SHG) \\ P(2\omega_2) &= \varepsilon_0 \chi^{(2)} E_2^2 && (SHG) \\ P(\omega_1 + \omega_2) &= \varepsilon_0 2\chi^{(2)} E_1 E_2 && (SFG) \\ P(\omega_1 - \omega_2) &= \varepsilon_0 2\chi^{(2)} E_1 E_2^* && (DFG) \\ P(0) &= \varepsilon_0 2\chi^{(2)} (E_1 E_1^* + E_2 E_2^*) && (OR), \end{aligned}$$

where the labels refer to physical processes as follows: second-harmonic generation (SHG), sum-frequency generation (SFG) and difference-frequency generation (DFG). A special case of DFG when $\omega_1 = \omega_2$ is optical rectification (OR). This is a process where a static electric field is created within the nonlinear crystal. Due to the complex notation, also respective negative frequency components exist containing however the same information about the generated nonlinear processes.[52]

The Poynting vector $\mathbf{S}$ represents the energy flux and it is defined as

$$\mathbf{S} = \mathbf{E} \times \mathbf{H}. \tag{3.4}$$

The effect called walk-off exists when the Poynting vectors of different polarization components of the beam propagate to different directions in the medium.

3.1 Phase matching

Several nonlinear processes can occur in a nonlinear crystal but without constructive interference of the produced light only minimal amount of the generated light can be observed. The wavevector mismatch Δk has to be minimized in order to effectively transform power from one frequency component to another. For the process of sum frequency generation $\omega_3 = \omega_1 + \omega_2$, Δk can be written as

$$\mathbf{\Delta k} = \mathbf{k_1} + \mathbf{k_2} - \mathbf{k_3}. \tag{3.5}$$

The mismatch affects the second harmonic intensity according to

$$I(2\omega) = I_{\max}(2\omega) \frac{\sin^2(\Delta k l_c/2)}{(\Delta k l_c/2)^2} = I_{\max}(2\omega) \mathrm{sinc}^2(\Delta k l_c/2), \tag{3.6}$$

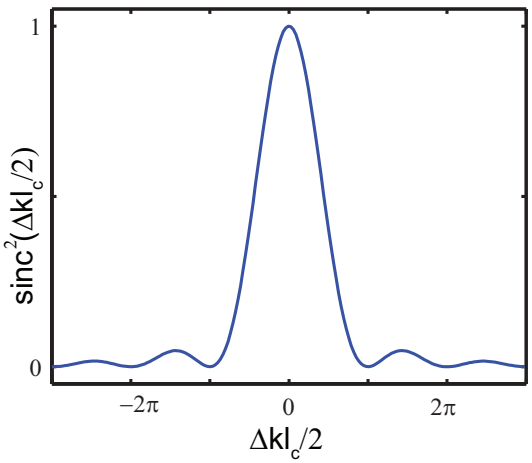

Figure 3.1. Effect of wavevector mismatch on the intensity in the sum frequency conversion.

where l_c is the length of the crystal. This equation is plotted in Figure 3.1. The conservation of energy in the sum frequency generation requires that

$$\hbar\omega_3 = \hbar\omega_1 + \hbar\omega_2. \tag{3.7}$$

With $k = 2\pi/\lambda = n\omega/c$, the phase matching requirement $\Delta k = 0$ becomes

$$\frac{n_1\omega_1}{c} + \frac{n_2\omega_2}{c} = \frac{n_3\omega_3}{c}. \tag{3.8}$$

This requirement in the special case of SHG is $n(\omega_1) = n(2\omega_1)$. For lossless materials, the refractive index increases with frequency (normal dispersion) and therefore this requirement is not fulfilled without special arrangements. Phase matching can be achieved by choosing the propagation direction so that the dispersion and birefringence effects cancel each other. In birefringent materials polarization can be divided to ordinary and extraordinary components. Ordinary component is perpendicular to the optical axis and the propagation vector **k**. Extraordinary component is perpendicular to the ordinary component and the propagation vector.

Two methods can be used to satisfy the phase-matching requirement. Incident beam can contain either ordinary or extraordinary polarization component, whereas the second harmonic field contains the other polarization component. This is called type-I phase matching. In type-II phase matching, the fundamental field is composed of both extraordinary and ordinary polarization components while the second harmonic contains

one component [52]. Type I phase matching is illustrated in Figure 3.2 where refractive indices for ordinary and extraordinary waves are drawn at the pump and second harmonic frequencies as a function of the incoming angle on the crystal. Phase matching is possible when $n(2\omega) = n(\omega)$.

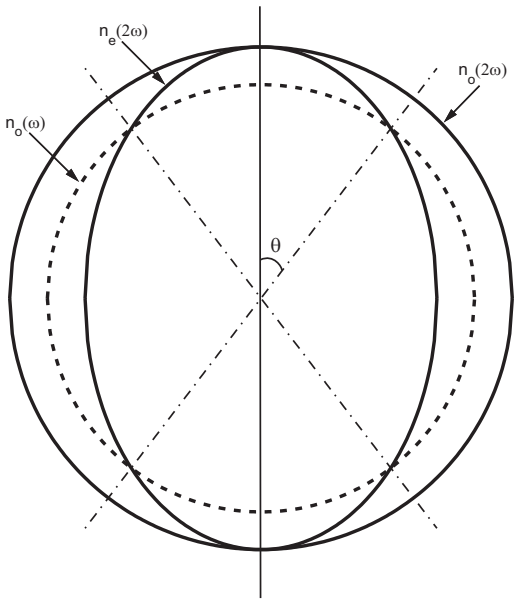

Figure 3.2. Ordinary (n_o) and extraordinary (n_e) refractive indices for pump (dashed) and second harmonic frequencies (solid) for negative uniaxial crystal as a function of the incoming angle of the beam. Phase matching is possible at an angle θ where $n_e(2\omega) = n_o(\omega)$.

When walk-off exists is the phase matching critical which is typical for angle phase matching. When there is no Poynting vector walk-off, the phase matching is called noncritical [52]. In type II phase matching the walk-off can exist between the two polarization components that pump the nonlinear process. This places further requirements in optimizing the conversion[53]. In Publication II the frequency doubling of 946 nm was performed with a BiBO crystal with walk-off the of 40.7 mrad. The effect can be seen as an elongated beam profile in Figure 3.5 showing the measured and simulated[54] beam profiles.

It is possible to tune the refractive indices and thus also the phase-matching condition by adjusting the crystal temperature or the beam incoming to the crystal. In angle tuning the orientation of the nonlinear crystal is adjusted to the phasematched direction. This method enables

compact and energy efficient setup. Usually however, there exists some walk-off. The acceptance angle for a given nonlinear process goes down with increasing walk-off angle and therefore it affects also the optimal pump focusing. The angular acceptance value is large for the noncritically phasematched process. The effective nonlinear coefficient for the given nonlinear process is determined by the nonlinear tensor of the crystal and the phase-matching angle.

By changing the temperature of the nonlinear crystal it is possible to tune the refractive indices and thus also the phase-matching condition. It might also be possible to find a nonlinear crystal where a given nonlinear process would become noncritically phasematched. Temperature control requires extra electronics and heating. A practical lower limit to the temperature tuning range is usually set by water condensation temperature.

In quasi-phase-matching the phase matching is achieved by structural periodicity that is built into the nonlinear medium. This can be achieved by changing the sign or the magnitude of the nonlinear coefficient periodically. In bulk crystals the poling can be done by electric field poling of ferroelectric crystals where the periodicity is attained by exceeding the coercive field of the crystal with an external one. This has been first done with $LiNbO_3$ by Yamada *et al.* in 1993 [55].

One of the key concepts in the quasi-phase-matching is the coherence length l_{cl} which is the length after which two waves, starting at the same point with the same phase, have generated a mutual phase difference of π. This is the point where the nonlinearity has to be modulated in order to prevent destructive interference. An expression for the coherence length for the SHG process can be solved from equation

$$\pi = \Delta k l_{\mathrm{cl}} = (k_2 - 2k_1) l_{\mathrm{cl}}. \tag{3.9}$$

Inserting the wave numbers for the fundamental and second harmonic waves $k_1 = 2\pi n_1/\lambda_1$ and $k_2 = 2\pi n_2/\lambda_2$ and solving for l_{cl} gives

$$l_{\mathrm{cl}} = \frac{\lambda_1}{4(n_2 - n_1)}. \tag{3.10}$$

There is no walk-off for a QPM process. The technique can enable phase matching of materials that can not be phasematched using birefringent phase matching. Also for some materials like $LiNbO_3$ it is possible to get

access to the highest nonlinearity element at the nonlinearity tensor which requires the same polarization for all of the interacting waves. This is impossible using birefringent phase matching[52]. The effective nonlinearity is $2/\pi$ times the nonlinearity for the completely phasematched case [56]. Most often used nonlinear crystals for periodical poling are lithium niobate $LiNbO_3$[57], lithium tantalate $LiTaO_3$ [58, 59] and potassium titanyl phosphate $KTiOPO_4$ [60].

3.2 Optimum focusing in SHG

For optimal critical second harmonic generation, the pumping beam is elliptic. In practice, for circular beams, the extra lens or lenses that are required to achieve the optimal beam size introduce losses and the alignment becomes more demanding. These difficulties can cancel the benefits of optimal elliptic focusing. When the processes of frequency-doublings and mixings are in cascade as is the case for frequency tripling or quadrupling, the beams can be elliptic caused by walk-off of the first conversion step and focusing becomes necessary separately in each direction of the elliptic principal axes. The optimum focusing parameter ξ can be determined from a graph in the classic publication by Boyd and Kleinman[61] with the help of a parameter

$$B = \frac{\rho\sqrt{l_c k_1}}{2}, \tag{3.11}$$

where ρ is the walk-off angle and k_1 is the wave number in the medium

$$k_1 = \frac{2\pi n}{\lambda_1}. \tag{3.12}$$

The parameter B is thus defined by the physical properties of the crystal and the specific nonlinear process. Without walk-off ($B = 0$) optimal ξ gets the value of 2.84. In the case of elliptic focus, the optimal focusing parameter values ξ for the both axes can be determined, from which the optimal $1/e^2$ waist value can be determined according to [62]

$$w_0 = \sqrt{\frac{l_c \lambda_0}{\xi 2\pi n}}. \tag{3.13}$$

As an example from Publication II, optimal focusing for SHG at 473 nm in a 10 mm long BBO crystal corresponds to the parameters n=1.68, and ρ=80.54 mrad. B-parameter gets the value 19 and 0 for walk-off and nonwalk-off directions, respectively and the optimal FWHM waist diameters are 56 μm and 14 μm.

The power of the second harmonic beam for low conversion can be calculated as

$$P_{\mathrm{SHG}} = K l_c k_\omega P_F^2 h e^{-\alpha l_c}, \tag{3.14}$$

with the coupling constant

$$K = \frac{2\omega^2 d_{\mathrm{eff}}^2}{\pi n_{2\omega} n_\omega^2 \epsilon_0 c^3}, \tag{3.15}$$

where h is the focus dependent value (Boyd-Kleinman factor) [61] and α is the absorption coefficient. The following formula for the conversion efficiency takes also into account the fact that the significant part of the fundamental power is converted to the second harmonic component. This is called the pump depletion [63]. The conversion factor η in the case of efficient conversion is

$$\eta(P_{\mathrm{F}}) = \tanh^2\left[\left(K l_c k_\omega P_{\mathrm{F}} h e^{-\alpha l_c}\right)^{1/2}\right] \tag{3.16}$$

with the second harmonic power being

$$P_{\mathrm{SHG}} = \eta(P_{\mathrm{F}})\ P_{\mathrm{F}}. \tag{3.17}$$

The effect of pump depletion is illustrated in Figure 3.3 for the SHG process of 946 nm and pulses with the peak power of 3.5 kW. The Boyd and Kleinman-factor h is 0.1, d_{eff} is 3.34 pm/V, and n is 1.8 for both wavelengths. The second harmonic power is 1.2 kW.

The simulated pulse energy conversions for the process from 946 to 473 nm in BIBO crystal for spherical and elliptical beams are shown in Figure 3.4 as a function of the pump beam diameter[54]. Simulations are made with 5 ns pulses with the peak power of 3.5 kW. The pulse energy is 17.5 μJ. The simulated and measured beam profiles are shown in Figure 3.5. One can notice the elongated shape of the second harmonic beam because of the walk-off of 40.7 mrad. The best simulated conversion of 34% is obtained with a FWHM waist diameter of 28 μm. This simulation

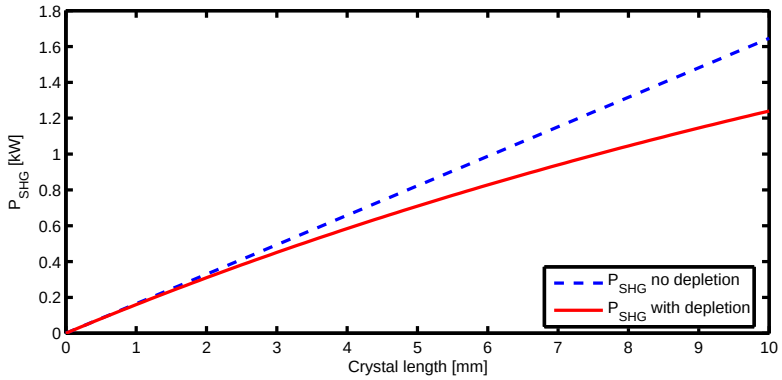

Figure 3.3. The effect of pump depletion for a 10-mm long BiBO crystal with h=0.1, d_{eff} =3.34 pm/V, and $n = 1.8$ for both wavelengths.

result is in agreement with the theory presented earlier. The conversion for elliptical focusing is 37% for the beam size of 28 and 17 μm to walk-off and nonwalk-off directions, respectively.

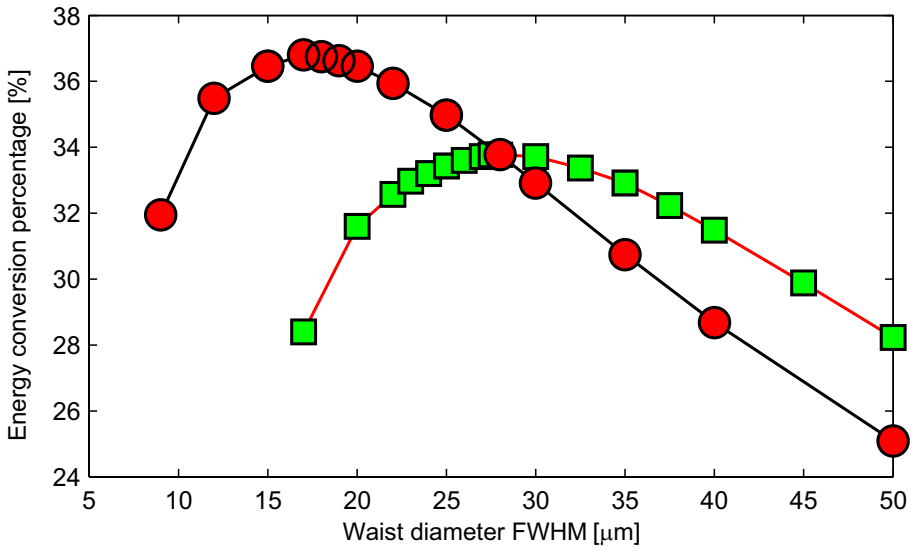

Figure 3.4. Calculated SHG pulse energy conversion as a function of the beam diameter (FWHM) for spherical (squares) and elliptical (circles) pump beams. For elliptical simulations the walk-off direction diameter is 28 μm and nonwalk-off direction is changed [54]. Pump pulse energy is 17.5 μJ and pulse width 5 ns.

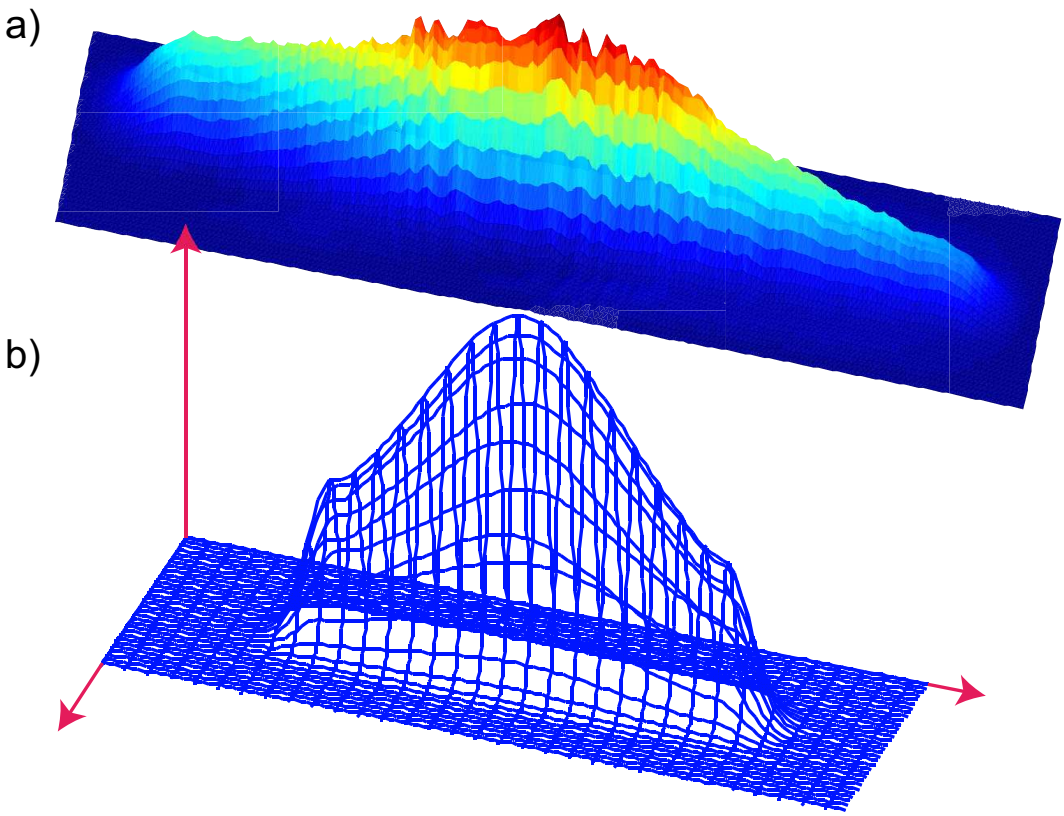

Figure 3.5. Measured (a) and simulated [54] (b) intensity beam profile at 473 nm.

3.3 Nonlinear crystals

Usually there exist various alternative nonlinear crystals that can be used for a given nonlinear process. The optimized properties for the output beam can be for example beam quality or output power. Important parameters for the process to consider are effective nonlinearity and walk-off. For optimal conversion efficiency the pump focus size becomes larger with increasing walk-off due to the pumping beam walk-off (type-II) or the reduced angular acceptance. Walk-off reduces also the beam quality for the walk-off direction and makes the beam elliptic. The mechanical, optical and chemical properties might place some extra limitations to the choice of the crystal (for example hygroscopicity, absorption or hardness).

Information on the nonlinear processes with different crystals that have been used in the experimental work in this thesis has been gathered to Ta-

ble 3.1. The relation between nonlinearity and second order susceptibility value is $d = 0.5\chi^{(2)}$.

Table 3.1. Phase-matching parameters for the nonlinear crystals and processes used in this thesis[54].

process crystal	λ_1 [nm] + walk-off[mrad]	λ_2 [nm] =	λ_3[nm]	length[mm] d_{eff}[pm/V]
SHG	946(e)	946(e)	473(o)	10
BIBO	40.7	40.7	0	3.3
SHG	473(o)	473(o)	236.5(e)	10
BBO	0	0	80.54	1.5
SHG	1123(e)	1123(o)	561(e)	5
KTA	2.35	0	3.0	3.25
SFG	1123(e)	561(e)	374.1(o)	6
BIBO	59.6	62.3	0	3.83
SHG	561(o)	561(o)	280.5(e)	10
BBO	0	0	84.5	1.82

The production of light via nonlinear conversion gets more demanding towards shorter wavelenghts. Many nonlinear crystals that are used to produce light at visible wavelengths absorb at UV. The available crystals have low nonlinearity (LBO), high walk-off (BBO) or poor mechanical or chemical properties (CLBO). The use of QPM becomes also difficult towards short wavelengths because the coherence length gets very short which makes the poling technically demanding. This trend can already be seen when the SHG process from 1064 and 946 nm to to green or blue are considered; the poling period gets from 6.8 to 4.6 μm for lithium niobate (LN) and from 9.2 to 6.1 μm for kalium titanium phosphate (KTP) at SHG of 1064 and 946 nm, respectively.

3.4 Raman scattering

The spontaneous Raman scattering was discovered in 1928 by C. V. Raman who got the Nobel prize for this discovery in 1930. In Raman scattering the incoming photon interacts with a phonon of the medium. The

energy of the scattered photon is shifted by the phonon energy. The loss of energy due to this process is called Raman Stokes scattering while also the increase of energy due to the Raman anti-Stokes scattering is possible. In Stokes scattering a transition occurs from ground state 1 to the final state 2, via virtual intermediate level associated with excited state 3. Anti-Stokes scattering includes transitions from 2 to 1 via virtual state close to level 3. A schematic picture of the energy levels of these two processes is shown in Figure 3.6. Stokes scattering is typically orders of magnitude more intense than the anti-Stokes effect due to the thermal equilibrium. The spontaneous Raman scattering is typically a weak process[52]. With intense optical fields stimulated Raman scattering (SRS) can be an efficient process which is demonstrated in the UV wavelength range in a pure silica core fiber in Publication IV where the SRS threshold is reached with laser pulses in a fiber with a 2-μm width core and length of 30 m. The stimulated Raman scattering builds up from two processes that reinforce each other. The spontaneous Raman scattering occurs at wavelengths that satisfy the conditions

$$\omega_S = \omega_L - \omega_v \text{ and } \omega_a = \omega_L + \omega_v, \tag{3.18}$$

where ω_S is the Stokes frequency, ω_a the anti-Stokes frequency, ω_L the laser pump frequency and ω_v the vibration frequency of the molecules. The beat frequency of ω_L and ω_S leads to the amplification of vibrations of the molecules which again reinforce scattering processes[52]. Spontaneous Raman scattering has a radiation pattern of a dipole[64], while stimulated Raman scattering leads to emission in a narrow cone in the forward and backward directions.[52]

Stimulated Raman scattering can be used to generate light and build lasers at wavelengths that are not directly available from solid state laser materials. With cascaded SRS it is possible to reach wavelengths further away from the pump wavelength.[23]

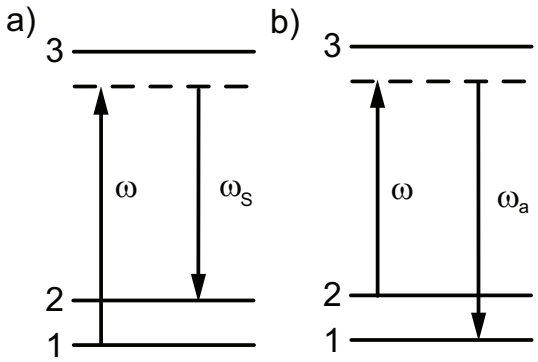

Figure 3.6. Energy level diagram of a) Raman Stokes scattering b) Raman anti-Stokes scattering.

4 Experimental results

4.1 Passively Q-switched 946 nm laser

The transition of Nd:YAG at 946 nm was used to produce high peak power laser pulses at IR in Publication I. In Publication II IR light was also converted to blue and UV wavelength ranges with a short pulse width. The wavelength of 236 nm was produced by cascaded single pass SHG conversions. Nonlinear crystals of BIBO and BBO were used to convert the light from IR to UV. In the laser of Publication I, we used a fiber coupled diode laser as a pump while in Publication II the laser was pumped by a laser diode stack. The size of elliptical blue beam focus in the BBO crystal was controlled by an elliptical and cylinder lenses. In Publication II for the nonlinear conversions the needed linear polarization was achieved by the thermal unisotropy introduced by the pumping laser diode. Peak powers of 2.7, 1.2 and 0.12 kW for the wavelengths of 946, 473 and 236 nm were achieved, respectively, with the UV pulse width of 1.9 ns.

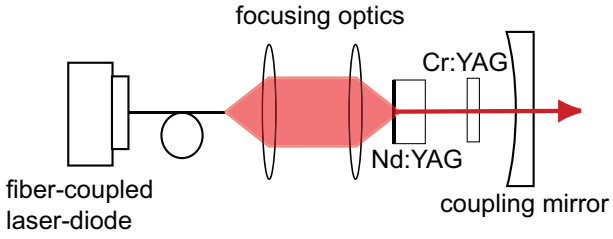

Figure 4.1. Schematic picture of the setup.

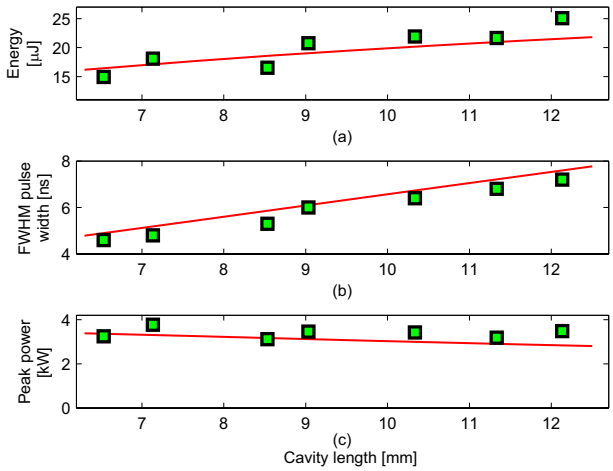

Figure 4.2. Pulse parameters as a function of the length of the cavity: (a) measured (squares) and calculated values (line) for pulse energy, (b) measured values (squares) and fitted line for the pulse length (FWHM) (c) peak power calculated from data of Figures (a) and (b).

4.2 Thermal tuning of pulse parameters

Stimulated emission cross section was changed by controlling the temperature of the laser crystal to tune the properties of passively Q-switched Nd:YAG laser at 1064 nm. The setup is presented in Figure 4.3. Time traces of the laser pulses for the different lasers presented in Publication III are drawn in Figure 4.4. The measured pulse properties as a function of the laser crystal mount and simulated laser crystal temperatures are presented in Figure 4.5.

4.3 Passively Q-switched laser at 1123 nm

Nd:YAG crystal has low gain transitions at 1112, 1116 and 1123 nm[23]. The transition at 1123 nm has been used to produce high peak power laser pulses at IR [IV-V]. These pulses have been converted to light at greenish yellow [IV-V] and at the UV wavelength ranges [IV]. The frequency conversions were done by using single pass schemes. Nonlinear crystals of KTA, BBO and BIBO were used to produce light at 561, 280 and 374 nm, with nonlinear processes of SHG, cascaded SHG and SHG followed by SFG, respectively. Spectral broadening of 374 nm pulses in a pure silica

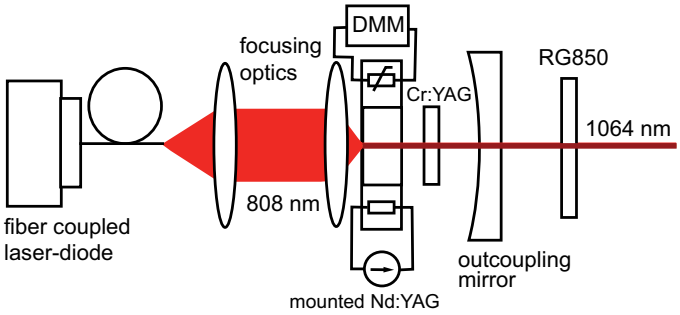

Figure 4.3. A schematic drawing of the pulsed Nd:YAG laser setup. Laser crystal mount is heated with a resistor. DMM refers to the digital multimeter that is used to measure the thermistor resistance that gives the temperature of the crystal mount and RG850 refers to a colored glass filter absorbing light at wavelengths below 850 nm.

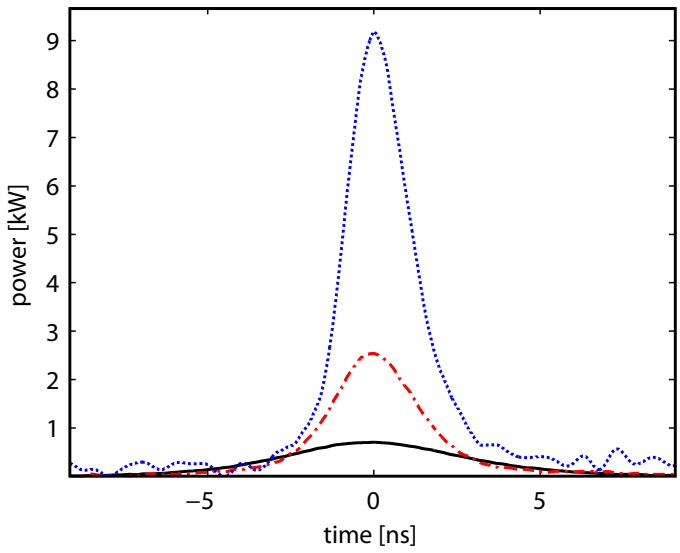

Figure 4.4. Time traces of the laser pulse power for the three lasers with no external heating of the crystal. Each pulse height was scaled to the measured peak power value. Solid: laser 1, dash dotted: laser 2, dotted: laser 3. The noise floor, due to limited signal to noise ratio, can be seen as ripple in the curve for the largest energy pulse.

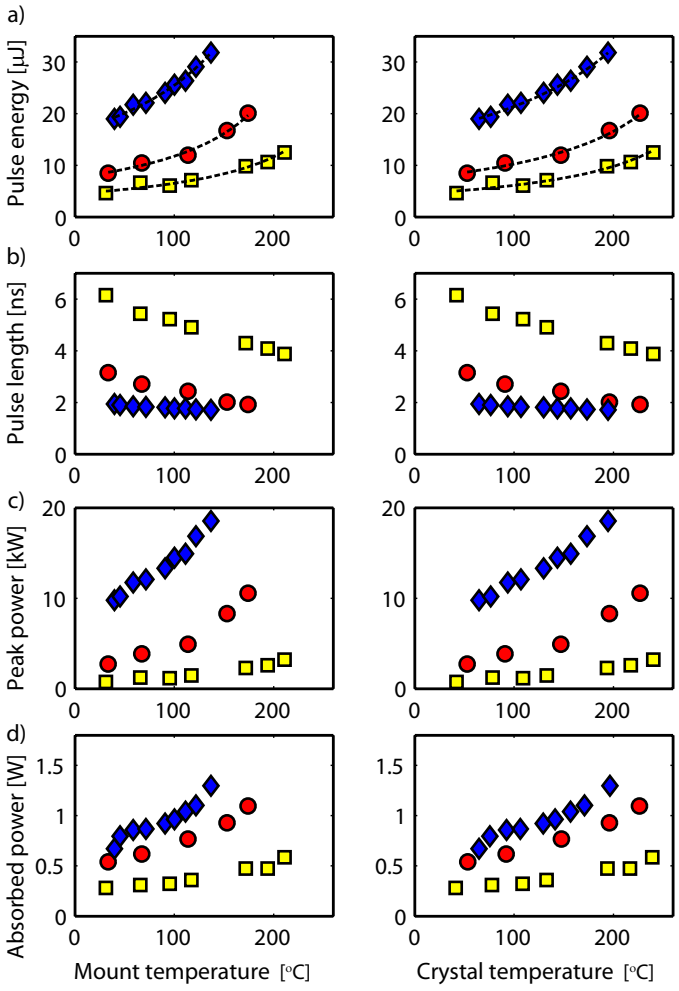

Figure 4.5. Measured laser pulse parameters as a function of the laser mount temperature and simulated laser crystal peak temperature: pulse energy (a), pulse length (b), peak power (c) and absorbed pump power at the laser threshold (d). Squares, circles and diamonds refer to lasers 1, 2 and 3, respectively.

core fiber was also studied utilizing effect of stimulated Raman scattering. Pulse parameters at different wavelengths are presented in Table 4.1. A picture of the setup is presented in Figure 4.6.

Table 4.1. Pulse parameters for pulses at wavelengths λ: average power P_{ave}, time between the pulses T_{per}, pulse energy E, pulse width FWHM T_{p} and peak power P_{p}.

λ [nm]	P_{ave} [mW]	T_{per} [μs]	E [μJ]	T_{p} [ns]	P_{p} [kW]
1123	282	142	40	12	3.2
561	55	156	8.6	8	1.0
374	16	155	2.5	8	0.31
280	3.8	161	0.61	6	0.10

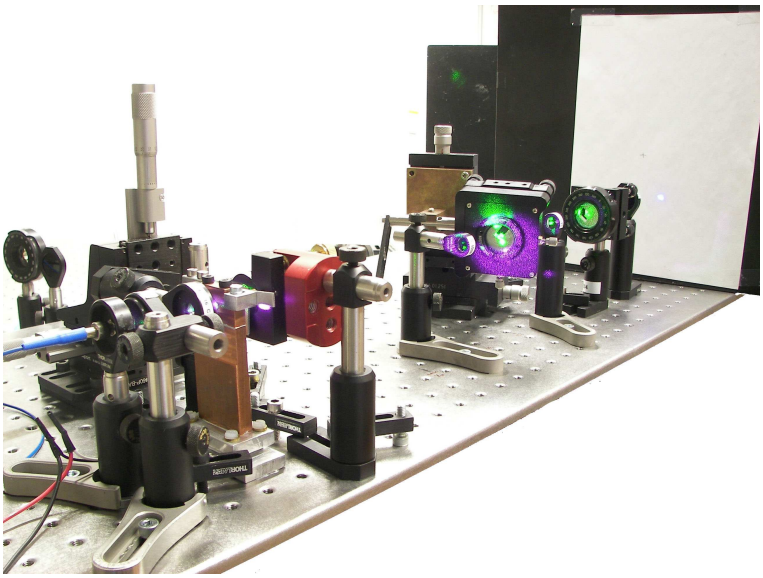

Figure 4.6. A picture of the laser setup for production of UV light at 280 nm.

5 Summary

This thesis presents research on passively Q-switched lasers. Furthermore, these laser sources have been used as pump sources to create light at visible and in the UV-wavelength ranges. The focus of this work has been in creating compact Nd:YAG lasers giving out short pulses with high peak power. A Cr:YAG crystal was chosen for passive Q-switching. These lasers are suitable for single pass nonlinear conversion which is a convenient and stable method to utilize a nonlinear process. The frequency conversions have been done by using birefringently phasematched nonlinear crystals.

Lasers that utilize low gain laser transitions have been studied, showing that also these laser transitions can be used to provide high peak power with short pulse width. Publications I and II report on highest peak power reported together with short pulses from a 946 nm laser and conversions to visible and deep UV wavelengths. The laser transition at 1123 nm corresponds to very low stimulated emission cross section and there are also other laser transitions nearby at 1112 and 1116 nm. Publications IV and V report a superior performance of passively Q-switched laser when compared to earlier reports with frequency conversions all the way to UV using birefringent phasematching. In addition to the low stimulated emission cross section, the 946 nm laser transition laser provides challenges due to the quasi-three-level laser transition.

UV-lasers are typically either bulky, very complex or they have low output power. The UV-lasers presented in this thesis are compact, robust and can provide decent average power in the mW range and peak powers at the 100 W range at wavelengths of 374, 280 and 236 nm.

A method of tuning the pulse properties of a passively Q-switched

laser is demonstrated showing a remarkable effect on the laser output. In this method, control of the laser crystal temperature is used to change the stimulated emission cross section. The experiments were carried out using a 1064 nm laser but the method can also be applied to other solid state four-level lasers. Furthermore, this study reports on dramatic effects of the crystal temperature on the laser pulses. Some of these effects are caused non-intentionally due to for example inadequate thermal conduction.

References

[1] A. Einstein "Zur Quantentheorie der Strahlung," Phys. Z. **18** 121-128 (1917).

[2] A. M. Prochorov "Quantum electronics" Nobel lecture in 1964, `http://nobelprize.org/nobel_prizes/physics/laureates/1964/`

[3] Official web site of the Nobel Foundation `http://nobelprize.org`

[4] T. H. Maiman "Stimulated optical radiation in Ruby," Science **187** 493 - 494 (1960).

[5] P. A. Franken, A. E. Hill, C. W. Peters, and G. Weinreich "Generation of Optical Harmonics," Phys. Rev. Lett. **7** 118 - 119 (1961).

[6] U. Keller, K. J. Weingarten, F. X. Kärtner, D. Kopf, B. Braun, I. D. Jung, R. Fluck, C. Honninger, N. Matuschek, and J. A. derAu "Semiconductor Saturable Absorber Mirrors (SESAM's) for Femtosecond to Nanosecond Pulse Generation in Solid-State Lasers," IEEE J. Sel. Top. Quantum Electron. **2** 435 - 453 (1996).

[7] M. Arvidsson "Far-field timing effects with passively Q-switched lasers," Opt. Lett. **26** 196 - 198 (2001).

[8] H. Ailisto, V. Heikkinen, R. Mitikka, R. Myllyla, J. Kostamovaara, A. Mantyniemi, and M. Koskinen "Scannerless imaging pulsed-laser range finding," J. Opt. A-Pure Appl. Opt. **4** S337 - S346 (2002).

[9] H. Schneckenburger, H. K. Seidlitz, and J. Eberz "New trends in photobiology (invited review) - Time-resolved fluorescence in photobiology," J. Photochem. Photobiol. B-Biol. **2** 1 - 19 (1988).

[10] P. Vita, N. Kurilcik, S. Jursenas, A. Zukauskas, A. Lunev, Y. Bilenko, J. Zhang, X. Hu, J. Deng, T. Katona, and R. Gaska "Deep-ultraviolet light-emitting diodes for frequency domain measurements of fluorescence lifetime in basic biofluorophores," Appl. Phys. Lett. **87** 084106 (2005).

[11] C. D. McGuinness, K. Sagoo, D. McLoskey, and D. J. S. Birch "A new sub-nanosecond LED at 280 nm: application to protein fluorescence," Meas. Sci. Technol. **15** L19 - L22 (2004).

[12] N. Kurilcik, P. Vitta, A. Zukauskas, R. Gaska, A. Ramanavicius, A. Kausaite, and S. Jursenas "Fluorescence detection of biological objects with ultraviolet and visible light-emitting diodes," Opt. Appl. **36** 193 - 198 (2006).

[13] S. Chadha, R. Manoharan, P. Moënne-Loccoz, W. H. Nelson, W. L. Peticolas, and J. F. Sperry "Comparison of the UV resonance Raman spectra of bacteria, bacterial cell walls, and ribosomes excited in the deep UV," Appl. Spectrosc. **47** 38 - 43 (1993).

[14] D. Ilie, C. Mullan, G. M. O'Connor, T. Flaherty, and T. J. Glynn "Controlled process for polymer micromachining using designed pulse trains of a UV solid state laser," Appl. Surf. Sci. **254** 845 - 849 (2007).

[15] S. Suihkonen, O. Svensk, P. T. Törmä, M. Ali, M. Sopanen, H. Lipsanen, M.A. Odnoblyudo, and V.E. Bougrov "MOVPE growth and characterization of InAlGaN films and InGaN/InAlGaN MQW structures," J. Cryst. Growth **310** 1777 - 1780 (2008).

[16] W. Bäumler, E. T. Eibler, U. Hohenleutner, B. Sens, J. Sauer, and M. Landthaler "Q-

switch laser and tattoo pigments: First results of the chemical and photophysical analysis of 41 compounds," Lasers Surg. Med. **26** 13 - 21 (2000).

[17] E. F. Bernstein "Laser treatment of tattoos," Clin. Dermatol. **24** 43 - 55 (2006).

[18] P. W. Milonni and J. H. Eberly "Lasers" John Wiley Sons, Inc. 1988

[19] O. Svelto, translated and edited by D. Hanna "Principles of Lasers," 4th edition, Plenum Press, New York, 1998.

[20] S. Bjurshagen, R. Koch, and F. Laurell "Quasi-three-level Nd:YAG laser under diode pumping directly into the emitting level," Opt. Commun. **261** 109 - 113 (2006).

[21] V. Lupei, G. Aka, and D. Vivien "Highly efficient, 0.84 slope efficiency, 901 nm, quasi-two-level laser emission of Nd in strontium lanthanum aluminate," Opt. Lett. **31** 1064 - 1066 (2006).

[22] M. E. Innocenzi, H. T. Yura, C. L. Fincher, and R. A. Fields "Thermal modeling of continuous-wave end-pumped solid-state lasers," Appl. Phys. Lett. **56** 1831 - 1833 (1990).

[23] W. Koechner "Solid-State Laser Engineering," 5th edition, Springer, Berlin, 1999.

[24] X. Y. Peng, A. Asundi, Y. H. Chen, and Z. J. Xiong "Heating measurements in diode-end-pumped Nd : YVO4 lasers," Opt. Eng. **40** 1100 - 1105 (2001).

[25] C. Czeranowsky, M. Schmidt, E. Heumann, G. Huber, S. Kutovoi, and Y. Zavartsev "Continuous wave diode pumped intracavity doubled Nd : GdVO4 laser with 840 mW output power at 456 nm," Opt. Commun. **205** 361 - 365 (2002).

[26] T. Pollak, W. Wing, R. Grasso, E. Chicklis, and H. Jenssen "CW laser operation of Nd:YLF," IEEE J. Quantum Electron. **18** 159 - 163 (1982).

[27] S. Guy , C. L. Bonner, D. P. Shepherd, D. C. Hanna, and A. C. Tropper "High-inversion densities in Nd : YAG: Upconversion and bleaching," IEEE J. Quantum Electron. **34** 900 - 909 (1998).

[28] S. Singh, R. G. Smith, and L. G. Van Uitert "Stimulated-emission cross section and fluorescent quantum efficiency of Nd3+ in yttrium aluminum garnet at room temperature," Phys. Rev. B **10** 2566 - 2572 (1974).

[29] A. E. Siegman "Lasers," 1st edition, University Science Books, Mill Valley, California, 1986.

[30] S. Amano and T. Mochizuki "Propagation characteristics of a diffracted M-2 beam," Appl. Optics **41** 6325 - 6331 (2002).

[31] A. E. Siegman, G. Nemes, and J. Serna "How to (Maybe) Measure Laser Beam Quality," in DPSS (Diode Pumped Solid State) Lasers: Applications and Issues, M. Dowley, ed., Vol. 17 of OSA Trends in Optics and Photonics (Optical Society of America), paper MQ1 (1998).

[32] H. Kogelnik and T. Li "Laser beams and resonator," Appl. Opt. **5** 1550 - 1567 (1966).

[33] T. Fan "Aperture guiding in quasi-three-level lasers," Opt. Lett. **19** 554 - 556 (1994).

[34] J. Salin and J. Squier "Gain guiding in solid-state lasers," Opt. Lett. **17** 1352 - 1354 (1992).

[35] E. J. Grace, G. H. C. New, and P. M. W. French "Simple ABCD matrix treatment for transversely varying saturable gain," Opt. Lett. **26** 1776 - 1778 (2001).

[36] J. K. Jabczynski, J. Kwiatkowski, and W. Zendzian "Modeling of beam width in pas-

sively Q-switched end-pumped lasers," Opt. Express **11** 552 - 559 (2003).

[37] T. Fan, and R. Byer "Modeling and CW operation of a quasi-three-level 946 nm Nd:YAG laser," IEEE J. Quantum Electron. **23** 605 - 612 (1987).

[38] T. Fan, and R. Byer "Diode laser pumped solid-state lasers," IEEE J. Quantum Electron. **24** 895 - 912 (1988).

[39] I. Lindsay and M. Ebrahimzadeh "Efficient continuous-wave and Q-switched operation of 946-nm Nd:YAG laser pumped by an injenction-locked broad area diode laser," Appl. Optics **37** 3961 - 3970 (1998).

[40] Y. Kalisky "Cr4+-doped crystals: their use as lasers and passive Q-switches," Prog. Quantum Electron. **28** 249 - 303 (2004).

[41] B. Cole, L. Goldberg, C. W. Trussell, A. Hays, B. W. Schilling, and C. McIntosh, "Reduction of timing jitter in a Q-Switched Nd:YAG laser by direct bleaching of a Cr^{4+}:YAG saturable absorber," Opt. Express **17** 1766 - 1771 (2009).

[42] J. Zayhowski and C. Dill III, "Diode-pumped passively Q-switched picosecond microchip lasers," Opt. Lett. **19** 1427 - 1429 (1994).

[43] H. Ridderbusch and T. Graf "Saturation of 1047-and 1064-nm absorption in Cr4+: YAG crystals," IEEE J. Quantum Electron. **43** 168 - 173 (2007).

[44] X. Y. Zhang, A. Brenier, J. Y. Wang, and H. J. Zhang "Absorption cross sections of Cr^{4+} : YAG at 946 and 914 nm," Opt. Mater. **26** 293 - 296 (2004).

[45] X. Zhang S. Zhao, Q. Wang, Q. Zhang, L. Sun, and S. Zhang, "Optimization of Cr^{4+}-Doped Saturable-Absorber Q-Switched Lasers," IEEE J. Quantum Electron. **33** 2286 - 2294 (1997).

[46] J. J. Degnan "Theory of the Optimally Coupled Q-Switched Laser," IEEE J. Quantum Electron. **25** 214 - 220 (1989).

[47] J. J. Degnan "Effects of thermalization on Q-switched laser properties," IEEE J. Quantum. Elect. **34** 887 - 899 (1998).

[48] S. P. Ng, D. Y. Tang, L. J. Qian, and L. J. Qin "Satellite Pulse Generation in Diode-Pumped Passively Q-Switched Nd:GdVO4 Lasers," IEEE J. Quantum. Elect. **42** 625 - 632 (2006).

[49] J. J. Zayhowski and P. L. Kelly, "Optimization of Q-Switched Lasers," IEEE J. Quantum Electron. **27** 2220 - 2225 (1991).

[50] J. J. Zayhowski and A. L. Wilson, Jr, "Pump-Induced Bleaching of the Saturable Absorber in Short-Pulse Nd:YAG/Cr^{4+}:YAG Passively Q-Switched Microcip Lasers," IEEE J. Quantum Electron. **39** 1588 - 1593 (2003).

[51] B. E. A. Saleh and M. C. Teich, "Fundamentals of Photonics," John Wiley & Sons, Inc. 1991.

[52] R. W. Boyd,"Nonlinear Optics," 3rd edition, Academic Press, New York 2008.

[53] J. Zondy "Comparative theory of walkoff-limited type-II versus type-I second harmonic generation with gaussian beams," Opt. Commun. **81** 427 - 440 (1991).

[54] SNLO version 41 nonlinear optics code available from A. V. Smith, Sandia National Laboratories, Albuquerque, NM 87185-1423.

[55] M. Yamada, N. Nada, M. Saitoh, and K. Watanabe "First-order quasi-phase matched LiNbO3 waveguide periodically poled by applying an external field for efficient blue

second-harmonic generation," Appl. Phys. Lett. **62** 435 - 436 (1993).

[56] M. M. Fejer, G. A. Magel, D. H. Jundt, and R. L. Byer,"Quasi-phase-matched second harmonic generation: tuning and tolerances," IEEE J. Quantum Electron. **28** 2631 - 2654 (1992).

[57] L. E. Myers, R. C. Eckardt, M. M. Fejer, R. L. Byer, W. R. Bosenberg, and J. W. Pierce "Quasi-phase-matched optical parametric oscillators in bulk periodically poled LiNbO3," J. Opt. Soc. Am. B-Opt. Phys. **12** 2102 - 2116 (1995).

[58] A. J. Tracy, C. Lopez, A. Hankla, D. J. Bamford, D. J. Cook, and S. J. Sharpe "Generation of high-average-power visible light in periodically poled nearly stoichiometric lithium tantalate," Appl. Optics **48** 964 - 968 (2009).

[59] J.-P. Meyn, C. Laue, R. Knappe, R. Wallenstein, and M. M. Fejer "Fabrication of periodically poled lithiumtantalate for UV generation with diode lasers," Appl. Phys. B **73** 111 - 114 (2001).

[60] C. Canalias, V. Pasiskevicius, R. Clemens, and F. Laurell "Submicron periodically poled flux-grown KTiOPO4," Appl. Phys. Lett. **82** 4233 - 4235 (2003).

[61] G. Boyd and D. Kleinman, "Parametric interaction of focused gaussian light beams," J. Appl. Phys. **39** 3597 - 3639 (1968).

[62] T. Freegarde, J. Coutts, J. Walz, D. Leibfried, and T.W. Hansch, “General analysis of type I second-harmonic generation with elliptical Gaussian beams,” J. Opt. Soc. Am. B-Opt. Phys. **14** 2010 - 2016 (1997).

[63] S. Spiekermann, F. Laurell, V. Pasiskevicius, H. Karlsson, and I. Freitag "Optimizing non-resonant frequency conversion in periodically poled media," Appl. Phys. B-Lasers Opt. **79** 211 - 219 (2004).

[64] R. W. Hellwarth "Theory of Stimulated Raman Scattering," Phys. Rev. **130** 1850 - 1852 (1963).

ISBN 978-952-248-073-6
ISBN 978-952-248-074-3 (PDF)
ISSN 1795-2239
ISSN 1795-4584 (PDF)